Instrument Science Report STIS 2013-03

Summary of STIS Cycle 18 Calibration Program

Gerard A. Kriss[1], Michael A. Wolfe[1], Alessandra Aloisi[1], K. Azalee Bostroem[1], Colin Cox[1], Van Dixon[1], Justin Ely[1], Chris Long[1], Elena Mason[1], Derck Massa[1], Rachel Osten[1], Charles Proffitt[2], Julia Roman-Duval[1], Paule Sonnentrucker[1], Thomas Wheeler[1], Wei Zheng[3]

[1] Space Telescope Science Institute, Baltimore, MD
[2] Computer Sciences Corporation
[3]Department of Physics & Astronomy, The Johns Hopkins University

20 November 2013

ABSTRACT

We summarize the Cycle 18 calibration program for the Space Telescope Imaging Spectrograph (STIS) on the Hubble Space Telescope covering the time period November 2010 through October 2011. We give an overview of the whole program, and status summaries for each of the individual proposals comprising the program.

Contents:

1. Introduction

The Space Telescope Imaging Spectrograph (STIS) on the Hubble Space Telescope was repaired in May 2009. Cycle 18 was the second cycle of on-orbit post-repair STIS operations. The calibration program for this period resembles the typical calibration and monitoring programs of the mature STIS instrument prior to its failure in 2004, with fewer special calibrations than had been included in the Cycle 17 STIS calibration program. Cycle 18 observations commenced in November 2010 and ran through October 2011. During this cycle there were a small number of lost observations due to the SIC&DH hang-up in September 2011; none had any relevant impact on the regular monitoring programs. Three observations were withdrawn due to scheduling issues. One observation failed due to a guide star acquisition failure but was repeated.

In this document we record and summarize the results of the individual calibration programs. Section 2 gives a summary and overview of the calibration program, which comprises 21 unique programs. Of these, 20 are regular programs to monitor and track instrument performance. One special calibration program is devoted to obtaining data for a new flux calibrator. Section 3 of this document details results from individual programs. The Appendix lists reference files and documentation produced as a result of Cycle 18 calibration programs.

2. Overview of Calibration Proposals for Cycle 18

Table 1 summarizes the orbit allocation and usage during the regular Cycle 18 calibration programs. No supplemental calibration programs beyond those proposed as the initial calibration plan were required for STIS in this cycle.

Table 1. Summary of orbit allocation and use during Cycle 18 STIS calibration.

	External Orbits		Internal + Parallel Orbits	
	Regular	**Supplemental**	**Regular**	**Supplemental**
Allocated	22	0	1370	0
Executed	23	0	1367	0
Withdrawn	0	0	3	0
Failed	1	0	8	0
Repeated	1	0	0	0

The calibration monitoring programs in Cycle 18 are essentially continuations of the monitoring programs from the previous cycle. These include programs which assess the stability of the CCD: its read out noise, spurious charge, charge transfer efficiency (CTE), and growth of hot pixels, and which also provide daily dark frames and bias frames for data processing and reduction. Other programs monitor the slit wheel repeatability, CCD and MAMA dispersion solutions, the MAMA focus, the MAMA fold distribution (i.e., the pulse-height distribution), and the sensitivity of both the CCD and MAMA detectors. For these programs, reference files are updated only as needed to maintain calibration within the required levels of accuracy.

Currently available reference files can be found at:
www.stsci.edu/hst/observatory/cdbs/SIfileInfo/STIS/reftablequeryindex
Other products resulting from the calibration program include STIS Instrument Science Reports (ISRs), STIS Technical Instrument Reports (TIRs), and updates to the STIS Instrument (IHB) and Data (DHB) Handbooks. Links to these documents can be found at:

www.stsci.edu/hst/stis/documents
Note that TIRs are only available on the internal STScI web site. In order to retrieve TIRs a document request needs to be sent to: **help@stsci.edu**

Table 2 provides a high level summary of the calibration programs, noting specifically products and accuracy achieved. The first two columns give the Proposal ID and its title; columns 3 and 4 give the number of executed [allocated] orbits for each proposal, divided into external and internal orbits. Column 5 gives the frequency of visits for monitoring programs. Column 6 describes the resulting products. For several programs, regularly updated reference files are produced. For many others, results are either posted on the web, or simply documented in Section 3 of this report. Column 7 gives the accuracy achieved by the calibration proposal. The last column of Table 2 notes the page in this ISR on which detailed information for that program can be found.

Table 2. Summary of Cycle 18 calibration and monitoring programs. Further details can be found in the following sections.

PID	Title	Orbits Used Executed[allocated]		Frequency	Products	Accuracy Achieved	Page
		External	Internal				
	CCD Monitors						
12396	CCD Performance Monitor		14[14]	2x7	CCD Reference File	<0.3 e^-	6
12400	CCD Dark Monitor, Part I		361[362]	365x1	Reference Files	S/N~1.34	8
12401	CCD Dark Monitor, Part II		368[368]	365x1	Reference Files	S/N~1.34	8
12402	CCD Bias & Read-Noise Monitor, Part I		180[181]	183x1	Reference Files	S/N~1.1—2.0	11
12403	CCD Bias & Read-Noise Monitor, Part II		183[184]	182x1	Reference Files	S/N~1.1—2.0	11
12404	CCD Hot-pixel Annealing		39P[39P]	13x3	Web Page Updates	See details in report	12
12405	CCD Spectroscopic Flats		37[37]	various	Reported in this ISR	<1.1% residual scatter	14
12406	CCD Imaging Flats		10[10]	various	Reported in this ISR	<0.2% residual scatter	16
12407	CCD Spectroscopic Dispersion Solution Monitor		3[3]	3x1	Reported in this ISR	Zero-points vary w/ rms <0.35 pixel	17
12408	CCD Sparse Field CTE		74[74]		Reported in this ISR	<1% for >200 e^-	21
12409	CCD Full-Field Sensitivity	1[1]		1x1	Reported in this ISR	0.3%	23
12410	Slit Wheel Repeatability		1[1]	1x1	Reported in this ISR	Repeatable to 0.02 pixels	25
12411	CCD Spectroscopic Sensitivity Monitor	6[5]		3x1/L, 1x2/M	TDS Reference File	<0.25% in rel. flux	28
	MAMA Monitors						
12412	MAMA Dispersion Solutions		7[7]	7x1	Reported in this ISR	Zero-points vary w/ rms <0.35 pixel	30
12413	MAMA Full-Field Sensitivity	3[3]		1x3	Reported in this ISR	FUV-MAMA: 0.3% NUV-MAMA: 2%	37
12414	MAMA Spectroscopic Sensitivity & Focus Monitor	12[12]		3x1/L, 1x1/M, 4x2/E	TDS Reference File	<0.6% in rel. flux	40
12415	MAMA Dark Monitor		116[116]	2/det/alt. wks + 2x6 FUV	Reported in this ISR	5—10%	42
12416	MAMA Fold Distribution		2[2]	1x2	Reported in this ISR	~5%	44
	MAMA NUV Flats		0	Cycle 19	None this cycle	N/A	—
12417	MAMA FUV Flats		11[11]		Reported in this ISR	<1.9% residual scatter	47
12429	MAMA Anomalous Recovery			contingency	N/A	N/A	49
	Special Programs						
12426	New COS FLUX Standard	1[1]			ISR	S/N~50 per 10 Å	51
	Totals	23[22]	1367[1370]				

P refers to pure parallel orbits.

3. Results from Individual Proposals

The following sections summarize the purpose, status, and results from the individual calibration proposals in the Cycle 18 program.

Proposal ID 12396: STIS CCD Performance Monitor (PI: Michael A. Wolfe)

Summary of Goals
This activity measures the baseline performance and commandability of the CCD subsystem. Bias and flat field exposures are taken in order to measure spurious charge, read noise, charge transfer efficiency (CTE) from the extended pixel edge response test (EPER), and gain. CCD performance measurements can be used to update the ccd parameters reference file if needed.

Execution
The execution of the program was nominal. Observations were taken every 6 months and consisted of 7 orbits. No changes were made to the program.

Summary of Analysis
The Read Out Noise (RON) and Gain has remained essentially the same throughout Cycle 18, see Tables 1 and 2. The spurious charge shows a decrease between March 2011 and September 2011, however the estimated values continue to be consistent with the variability seen in previous cycles (see Table 3). This behavior is seen with gain settings 1 and 4. The charge transfer inefficiency (CTI) as measured with the EPER test (note that this is a relative measure of CTI, not an absolute one) shows a slight increase in parallel CTI and a steady increase in serial CTI (see Table 4). Furthermore, the temperature dependence of the parallel and serial CTI is now clearly defined and can be seen in Figure 1. Statistics of sub-arrays used for target acquisitions show an increase in the mean value of counts for the 1024x32 sub-array during Cycle 18 (see Table 5).

Accuracy Achieved
Read noise error for all binning and gains is greater than 0.1 e- or ADUs. This is greater than the accuracy stated in the Phase I.

Reference Files Delivered
A new * ccd.fits was delivered with updated values for: CCD BIAS, READNSE, SPURCHARGE, and CTITIMFAC.

Relevent ISRs
None.

Continuation Plans
This program is continued in Cycle 19 as program 12740.

Supporting Details
See Figure 1 and Tables 1, 2, 3, 4, and 5.

Table 1. Gain and Read Noise (March 2011 data)

CCD Gain	xbin	ybin	Gain (e/ADU)	Gain Error (e/ADU)	RON (e-)	RON Error (e-)	Flux (e-)
1	1	1	1.00	0.01	5.65	0.26	18215.0
2	1	1	2.02	0.03	6.82	0.15	54919.0
4	1	1	4.13	0.03	8.33	0.30	77412.0

Table 2. Gain and Read Noise (September 2011 data)

CCD Gain	xbin	ybin	Gain (e/ADU)	Gain Error (e/ADU)	RON (e-)	RON Error (e-)	Flux (e-)
1	1	1	0.99	0.01	5.69	0.08	18204.0
4	1	1	4.10	0.05	8.78	0.41	77498.0
8	1	1	8.15	0.08	11.7	0.26	65063.0

Table 3. Spurious Charge

Date	Gain	CCD Position	Spurious Charge (e-)	Spurious Charge Error (e-)
March 2011	1	Row 512	1.34	0.725
March 2011	1	Row 900	0.840	0.589
March 2011	4	Row 512	7.11	1.41
March 2011	4	Row 900	6.63	1.31
September 2011	1	Row 512	1.21	0.708
September 2011	1	Row 900	0.736	0.574
September 2011	4	Row 512	6.81	1.37
September 2011	4	Row 900	6.33	1.27

Table 4. EPER CTI

Date	Parallel CTI	Parallel CTI Error	Serial CTI	Serial CTI Error
March 2011	0.0000839	0.00000143	0.00000726	0.00000009
September 2011	0.0000885	0.00000160	0.00000844	0.00000013

Table 5. Sub-Arrays

Date	Sub-Array Size	Mean (e-)	Standard Deviation (e-)	Median (e-)	S/N
March 2011	100x100	0.2012	0.6767	0.1235	0.2973
September 2011	100x100	0.2023	0.6787	0.0994	0.2981
March 2011	1024x32	0.2340	0.7089	0.2276	0.3301
September 2011	1024x32	0.3014	0.8306	0.2398	0.3629

Figure 1. Relationship between parallel and serial CTI as a function of CCD housing temperature. Note that the parallel CTI increases with increasing housing temperature and that the serial CTI decreases with increasing housing temperature (top and bottom plots, respectively). The data plotted is post-SM4.

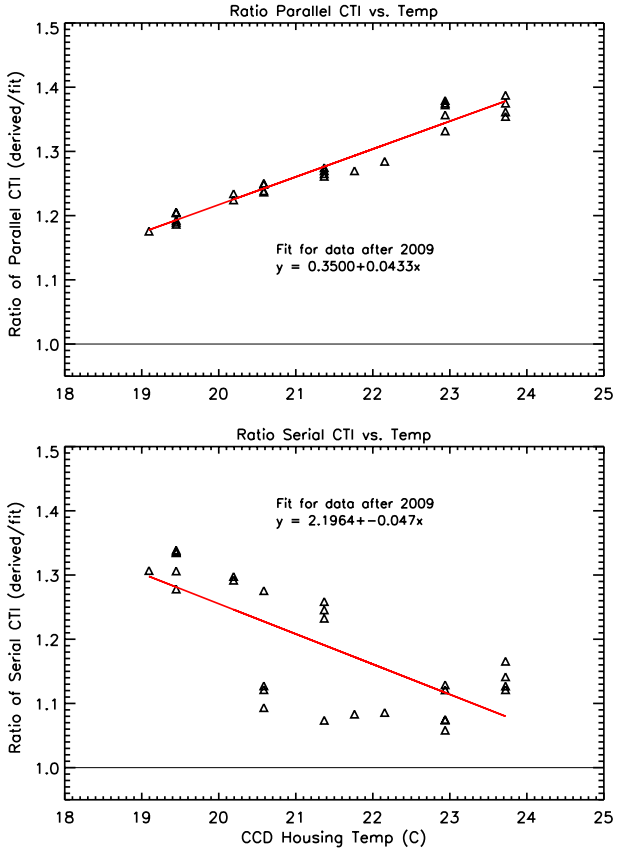

Proposal ID 12400 & 12401: CCD Dark Monitor Parts 1 & 2 (PI: Wolfe)

Analysis Lead, Others: Michael A. Wolfe, Van Dixon, and Justin Ely.

Summary of Goals
The goal was to produce weekly dark reference files from a series of long dark exposures (1100 s). Several short dark exposures (60 s) were taken daily for observers to use to update the hot pixel intensities in the weekly dark reference files using the STSDAS script daydarkT.cl.

Execution
729 out of 730 visits were executed. Visit 69 was withdrawn due to scheduling considerations. Additionally, visits 8D and 8E lost all data due to SIC & DH failure.

Summary of Analysis
Data taken between monthly anneals is combined to produce a baseline dark image. Weekly reference dark files are made by using weekly data to update the hot pixels in the baseline dark image. The bias reference image for the corresponding time range is used to remove the bias from the dark reference frame. The dark current continues to show increased scatter when compared to previous calibration cycles. Figure 1 demonstrates that the peak of the distributions of the dark current has increased. Figure 2 represents the behavior of the dark current as a function of time. There appears to be less scatter in the data as compared to Cycle 17 (see Figure 2) but the scatter remains significantly larger than it was prior to SM4. This increased scatter is probably a consequence of CCD damage due to irradiation, but additional analysis is required to fully characterize these changes and possible ameliorations.

Accuracy Achieved
The dark current ranged from 0.01375 to 0.01521 e-/s/pixel and the S/N of the superdarks are ≈ 1.34. There is an ongoing investigation into the scatter inherent in the dark current. Therefore, at this time, it is difficult to calculate a robust accuracy for the dark current.

Reference Files Delivered
4 superdarks were delivered each anneal period.

Relevent ISRs
None.

Continuation Plans
These two programs will be continued in Cycle 19 as programs 12741 and 12742.

Supporting Details
See Figures 1 and 2.

Figure 1. The black histogram is from a superdark taken at the beginning of Cycle 18 and the red histogram is of a superdark taken at the end of Cycle 18 calibrations. The time span is from November 1, 2010 to October 31, 2011.

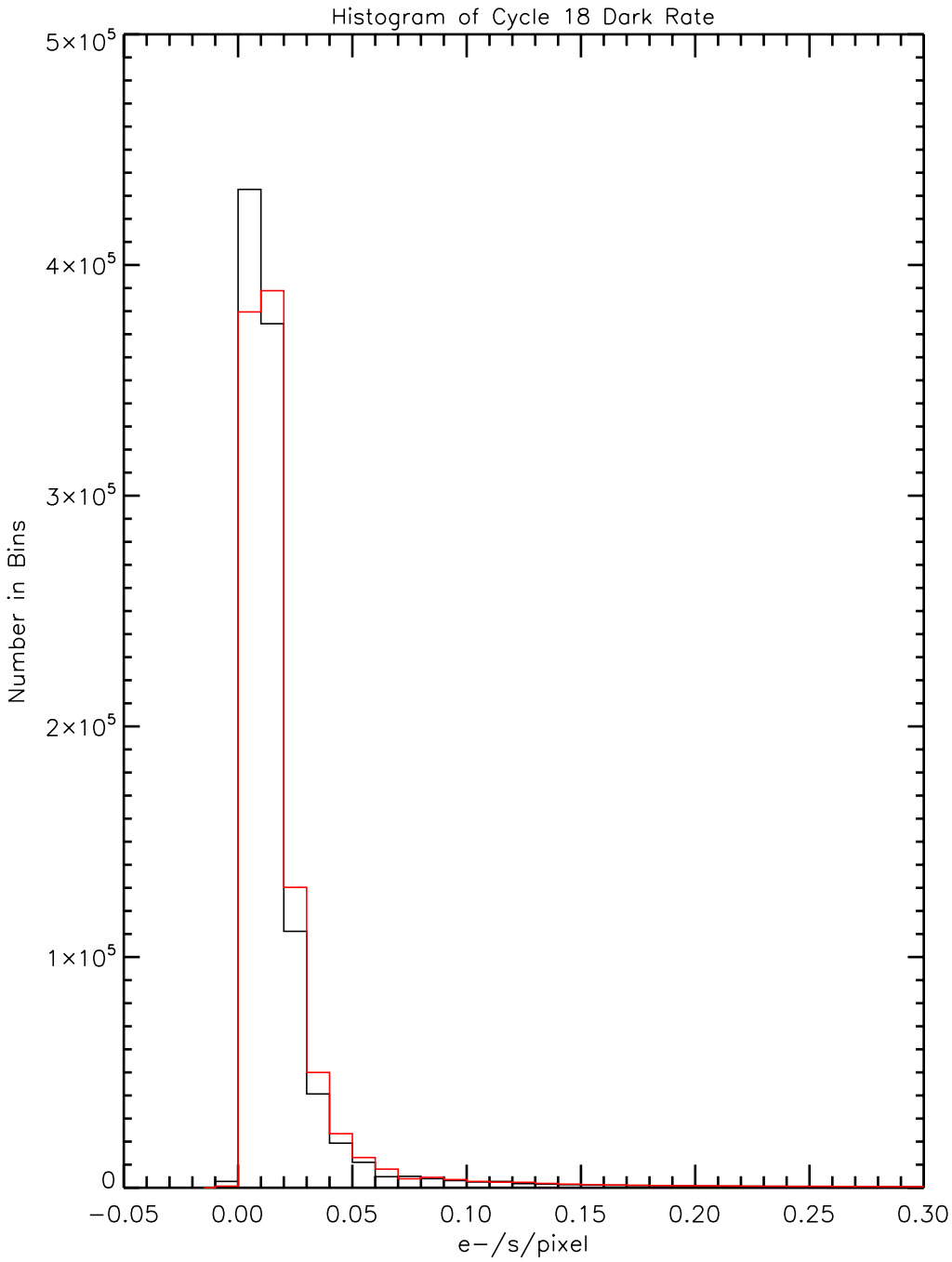

Figure 2. Plot of the median dark current as a function of time. Cycle 18 values can be found between the green and red vertical lines.

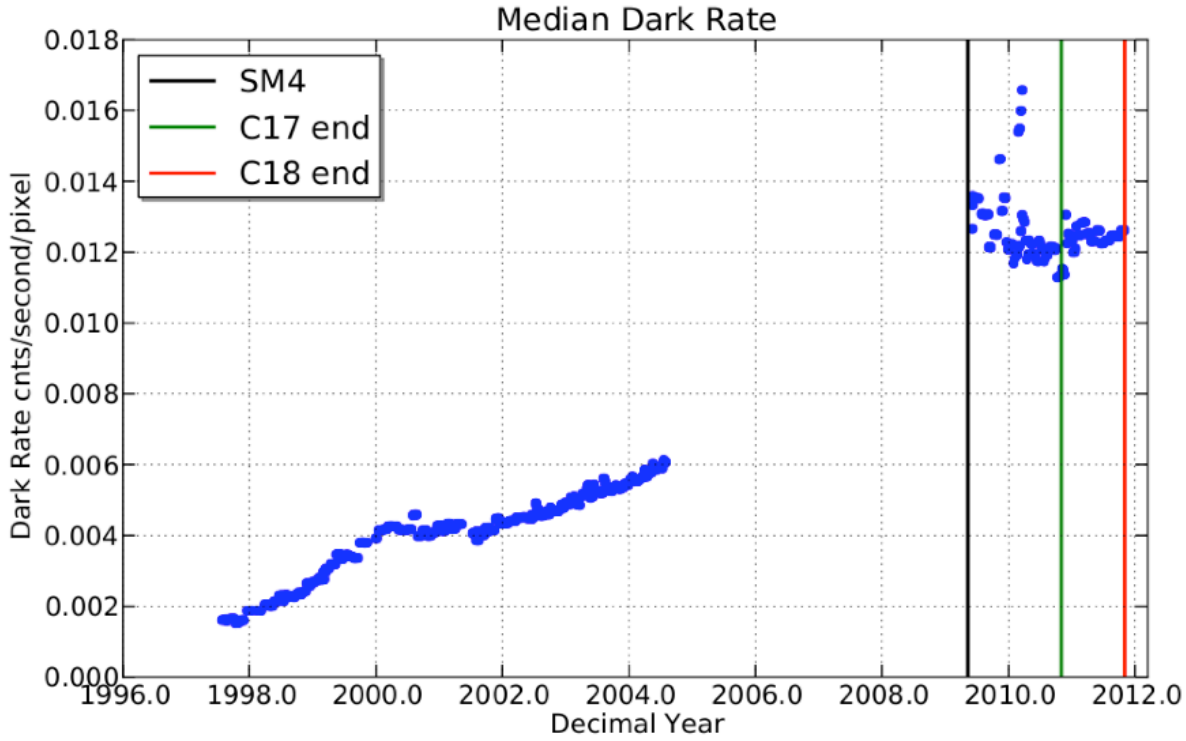

Proposal ID 12402 & 12403: CCD Bias and Readnoice Monitor Parts 1 & 2 (PI: Wolfe)

Analysis Lead, Others: Michael A. Wolfe, Van Dixon, and Justin Ely.

Summary of Goals
The goal was to produce bias reference files for gain 1(1x1 binning; weekly files) and gain 4 (1x1 binning; biweekly files), while achieving a signal to noise that is adequate to measure hot columns on these time scales. The evolution of read noise for gains 1 and 4 was also tracked.

Execution
363 out of 365 visits were executed. Visits 35 and 1U were withdrawn due to scheduling considerations. Additionally, visit 42 lost all data due to a SIC&DH anomaly. The lost and withdrawn visits contained only standard unbinned, AMP-D bias exposures, and so there was no need to repeat these visits.

Summary of Analysis
Data taken between monthly anneals is combined weekly or biweekly (gain = 4) to produce bias reference files. In most cases, within a given anneal week, there is enough data to produce a superbias with a S/N > 1.0. However, when there is not enough data, a baseline bias is created from all of the data within a pertinent anneal month. This baseline bias plus the weekly bias are then combined, thus providing good S/N monthly averages for the normal columns while updating the hot columns with the weekly data. Pairs of bias frames were used to measure the read noise by measuring the RMS dispersion in a difference image cleaned of discordant pixels via iterative sigma clipping. Over the course of Cycle 18, batch mode programs were run periodically to make the measurements and produce cumulative tables and plots. These were then used to produce routine updates of the STIS calibration monitor webpage (http://www.stsci.edu/hst/stis/performance/monitoring/). Means, medians, standard deviations, and S/N values derived from the superbiases can be found in Table 1. The average value of the read noise for gain = 1 is 5.62 ± 0.10 DN and for gain = 4 the read noise is 2.01 ± 0.04 DN.

Accuracy Achieved
This program was designed to achieve a signal-to-noise of at least 1 for each bias reference file. The achieved S/N is given in Table 1 for data taken from August 2009 to October 2010. Note that all S/N measurements are > 1.00.

Reference Files Delivered
6 superbiases were delivered each anneal period consisting of 4 gain = 1, 1x1 binning and 2 gain = 4, 1x1 binning.

Relevent ISRs
None.

Continuation Plans
These two programs are continued in Cycle 19 calibrations as programs 12743 and 12744.

Supporting Details: See Table 1.

Table 1. Reference File: Standard Deviation and Signal-to-Noise

Gain	Binning	Number of Exposures	Mean (DN)	Median (DN)	Standard Deviation	Median S/N per exposure
1	1x1	98	1.114	0.9895	0.8723	1.1344
		98	1.207	1.043	0.8992	1.1599
4	1x1	42	2.462	2.081	1.038	2.0048
		42	2.446	2.017	1.105	1.8253

Proposal ID 12404: CCD Hot Pixel Annealing (PI: Wolfe)

Analysis Lead, Others: Michael A. Wolfe, Van Dixon, and Justin Ely.

Summary of Goals
The goal of the program was to anneal hot pixels and monitor the growth of hot pixels by examining pre- and post-anneal dark images.

Execution
The execution of the program was nominal. All 39 orbits executed without a problem.

Summary of Analysis
Figures summarizing the anneal results are posted monthly on the STIS monitors page http://www.stsci.edu/hst/stis/performance/monitoring/. Since the Side-2 electronics do not contain a working temperature control circuit for the STIS CCD detector, the data are scaled to a common CCD housing temperature before statistics are computed. During the period of this program, there was an overall trend towards larger number of post-anneal hot pixels over time, as seen in Figure 1, but the number of hot pixels at the level of 0.1e-/s fluctated considerably between measurements, even after the correction for temperature fluctuations was applied, varying from 46390 (beginning of Cycle 18) to 42625 (end of Cycle 18). The cause of these fluctations is not fully understood, but may be related to the hot pixel tails that result from the decline in CTE caused by radiation damage, and/or imperfect corrections of variations in the local dark rate resulting in the temperature fluctuations. The number of post-anneal hot pixels at the 0.1 e-/s level was as high as 46390 during this program. The median dark current for this same period varied between 0.01403 and 0.01276 counts/pixel/second. Average growth rate of hot pixels is ≈ 4.09% per year.

Accuracy Achieved
For Cycle 18 data, the greater variation in the dark current caused by the damage to the CCD via irradiation makes it more difficult than it was for pre-SM4 data to determine the fraction of new hot pixels which are alleviated by the annealing process each month. Therefore, it is difficult to derive an accurate measurement for the hot pixel growth rate.

Reference Files Delivered
No reference files are created from the anneal monitoring.

Relevent ISRs
None.

Continuation Plans
This program has been continued in Cycle 19 as 12765.

Supporting Details
See Figure 1.

Figure 1. The number of hot pixels found after the CCD anneals are shown for various count rate thresholds. The scatter in the data is caused by individual pixels being less well behaved, possibly due to the accumulation of radiation damage.

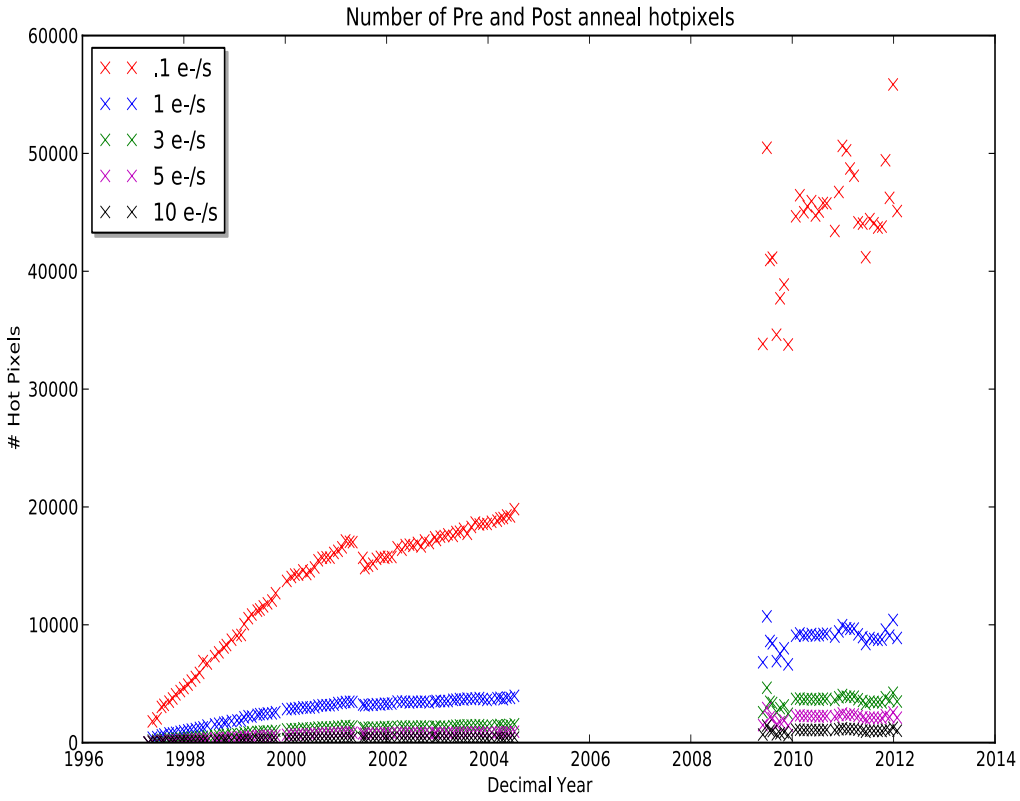

Proposal ID 12405: STIS CCD Spectroscopic Flat-field Monitor (PI: Elena Mason)

Analysis Lead, Others: Elena Mason

Summary of Goals
The primary goal was to determine the pixel to pixel variation for spectroscopic observations using the medium resolution (MR) grating G430M and the Tungsten lamp. The 50CCD and 52x2 apertures (at 5 different offset positions) are used in order to map the whole sensitive area of the detector.

In addition, spectroscopic flats where taken also with the G430L and the G750L gratings, in order to map the dust motes and blemishes in low resolution (LR).

MR and LR flats have p-flats that appear identical at most locations, but differences in the optical path and magnification between the different channels cause the images of the dust motes on the detector window to appear at different positions with different shapes. The map currently in use for the l-mode flats is outdated (dating back to 1999), as a few % "flux" difference has been reported for several dust motes.

Execution
9 orbits were used to gather flat field frames (each containing 9 imsets of 21 sec exptime) with the instrument setup G430M/50CCD. The orbits or visits were separated by about 41 days from each other, in order to monitor the stability. Similarly 10 more orbits were used to gather flat field frames (each containing 2 imset of 550 sec exptime) with the instrument setup G430M/52x2. Different visits had different slit offsets. The adopted offsets were: +7300, +3640, 0, -3640, -7300, so that for each offset there are a total of 4 frames or imsets. In this case all the visits where executed within an annealing period.

For the LR flat field, 5 orbits where used to collect frames with the G430L/50CCD instrument setup, 10 orbits with the G430L/52x2 (cycling across the different slit-offset listed above), and 3 orbits where spent to collect LR flat filed with the G750L/50CCD instrument setup.

All the visits were completed successfully with no failure of any type.

Summary of Analysis
The MR flats were processed, combined, normalized and further combined in a single pixel-to-pixel flat image (m-mode reference p-flat) using the existing python code. The code has been extensively compared with existing IDL scripts and modified to work on Cycle 18 MR data (whose projected shadow of the slit-bars has shifted). Various masking parameters have been tested in order to select the best result. The 50CCD flat was normalized applying a spline fit both along the columns (spline of order 3 with 25 nodes) and the rows (spline of order 3 with 13 nodes). Columns were median filtered (with box=13) before the spline fitting. The 52x2 flats were normalized applying a spline fit along the columns only (spline of order 3 with 13 nodes).

The resulting combined and normalized "master"/"super" flat has been compared with previous reference frames in the oref/ directory and in particular, with the reference flats delivered in 2009

and 2002. The ratio of the new m-mode p-flat with respect to the 2009 and 2002 reference frames show that there are no major differences apart from a larger masked area on the top part of the CCD.

The script also automatically produces an l-mode reference flat by simply taking the m-mode flat and replacing its dust motes with those appropriate for the LR grism magnification. However, this procedure uses an image of the l-mode dust motes which dates back to 1999. After SM4, it was noted that a few dust motes have shifted and/or differ by a few % with respect to the 1999 map. Hence the l-mode flat has been used to create a new l-mode p-flat. This was done, modifying as necessary the python script, and testing, again, several different parameters/options. In particular, the set of flats taken with the 52x2 slit have very low signal in the 300-500 left-most pixels of the detector which decreases the accuracy of the combined final p-mode flat. For this reason, the l-mode p-flat was created using only the flats taken with the 50CCD aperture. The 50CCD flats were normalized by spline fitting along the columns (3^{rd} order spline, 25 nodes and median filtering with box=15 before the fitting) and the rows (3^{rd} order spline with 13 nodes and no median filtering).

Accuracy Achieved

The new m-mode reference flat has MEAN and STDDEV of 0.9997 ± 0.01127 and 1.0 ± 0.00943, over the whole and central 100x100 pixels area of the detector, respectively. These values are consistent with those that can be measured in the existing reference frames and fulfill the 1% accuracy requirements.

The average differences in the ratio image between the new and the old reference m-mode p-flats are within 0.8% and 1.7%, for the 2002 and 2009 flat respectively.

The new l-mode p-flat has MEAN and STDDEV of 0.9995 ± 0.01006 and $1. \pm 0.00850$ in the whole and central area of the detector, respectively. These values are consistent with the 1% accuracy requirements and with past reference frames. The ratio image of the new l-mode p-flat with respect to the 1999 flat shows significant differences for several dust motes, while there are no significant differences at the 0.5% level in the smooth areas.

Reference Files Delivered

A new m-mode p-flat, valid for all the m-mode observations, has been delivered, and a new l-mode p-flat, valid for all the l-mode observations, has been delivered.

Relevant ISRs

"STIS CCD Spectroscopic P-flats", E Mason, ISR STIS 2013-05.

Continuation Plans

The spectroscopic flat monitoring program is continuing in Cycle 19, with PID number 12766 and no significant changes.

Supporting Details

N/A

Proposal ID 12406: STIS CCD Imaging Flat-field Monitor (PI: Elena Mason)

Analysis Lead, Others: Elena Mason

Summary of Goals
The goal of the program was to investigate the flat-field stability during a 1.5-month period and possibly map a few non-standard step-positions for 50CORON.

Imaging flats were taken at semi-regular interval across the cycle with the purpose of monitoring the CCD response and to map the possible development of defects. In addition, a set of imaging flats with the 50CORON mask was taken with the mask at an offset position.

Execution
8 orbits were dedicated to the gathering of imaging flats with the 50CCD and the F28X50LP apertures. For each instrument setup, 6 imsets of 0.1 sec exposure time were taken at each visit. The visits were distributed across the cycle and separated by ~7 weeks (1.5 months) from each other.

2 visits/orbits were intended to create a flat field with the 50CORON mask at an offset position. These two visits failed as the QUESIPARAM entry for the slit offset was specified with the wrong syntax (SLIT-STEP in place of SLITSTEP. Note that SLIT-STEP is the correct syntax for the OPTIONAL PARAMETER box in the APT) so that the flats have the 50CORON mask at the standard position.

Summary of Analysis
The stability of the CCD response within the cycle was checked by computing the average frame within each visit and the ratio of each average frame corresponding to visits $n \geq 2$ with respect to the 1st average frame (n=1), for each instrument setup.

In addition, all the frames collected within the program were combined in two "master" flats (one per each aperture) and compared with similar frames crated using the cycle 17 imaging flat field.

The master flat for the 50CCD setup has also been normalized (using a 2D median filter of 55x55 pixels) and compared with ground CCD MIRVIS clear aperture flat h4s1351lo_pfl.fits, in the oref/ directory.

Accuracy Achieved
When ratios of flats taken at different epochs during cycle 18 are inspected, one notices no significant difference at ~0.3% level in the central part of the detector. However, the illumination pattern may differ by more than 0.3% with respect to the average in the corner area of the 50CCD aperture.

When the combined master flats of Cycle 18 are compared with those of Cycle 17, one observes no significant structures at the $\leq$0.2% level.

When compared with h4s1351lo_pfl.fits in the calibration database, one observes no major structures at the 0.6% level in the central (200:800,200:800) part of the detector. There are about 6 dust motes which have shifted near the detector edges.

Reference Files Delivered
No revisions to existing calibration reference files are needed.

Relevant ISRs
None.

Continuation Plans
The program has been continued in Cycle 19 (PID 12767) with no significant changes with respect to cycle 18.

Supporting Details
N/A

Proposal ID 12407: CCD Spectroscopic Dispersion Solution Monitor (PI: Pascucci)

Analysis Lead, Others: Paule Sonnentrucker

Summary of Goals
The goal was to verify the STIS CCD dispersion solutions using internal HITM1 wavecal data for all 6 gratings supported for CCD spectroscopic observations. There were no external targets used.

Execution
The three 1-orbit visits of this yearly program executed on Nov 15, 2010. Data were successfully obtained using the G230LB, G230MB, G430L, G430M, G750L and G750M gratings. The 52x0.1" slit was used in all cases. No data loss occurred.

Summary of Analysis
The HITM1 lamp exposures were reduced with CalSTIS as if they were science exposures. The emission lines in the resulting x1d spectra were fitted with Gaussian profiles. The difference between the fitted line centroids and the corresponding laboratory wavelengths was computed for all identified lamp lines. For each mode the mean and standard deviation of the latter differences were then calculated.

Accuracy Achieved
The mean of the difference distribution is lower than 0.1 pixel and the standard deviation is lower than 0.3 pixel in all cases, except for the G230MB 2416 CENWAVE setting where the mean of difference is 0.2 pixel. This larger value is likely due to the small number of lines present in the range. These results are consistent with those reported for Cycle 17 by Pascucci et al. 2011 (ISR STIS 2011-01(v1)).

Reference Files Delivered
No new reference file needs to be delivered as the solution accuracy has not changed since Cycle 17 or since SM4.

Relevant ISRs
There is no need for publication of a new ISR.

Continuation Plans
The monitoring program for the CCD dispersion solution was carried over to Cycle 19 as Program 12768 for a total of 3 visits, each of 1 orbit, as in Cycle 18. The gratings and cenwaves used in Cycle 18 were also carried over to the Cycle 19 monitoring program.

Supporting Details
The figures and tables below give the mean and standard deviations derived from the monitoring data for each grating and cenwave combination.

Table 1. Summary of achieved accuracy for G230LB and G230MB.

Grating-Cenwave	Mean Offset (pix)	Standard Deviation (pix)
G230LB-2375	0.02	0.29
G230MB-1713	0.02	0.30
G230MB-1995	0.08	0.28
G230MB-2416	0.13	0.10
G230MB-2697	0.06	0.35
G230MB-3115	-0.06	0.09

Figure 1. The achieved accuracies in Cycle 18 are consistent with those derived in Cycle 17 and fulfill the requirements for the CCD gratings and M mode combinations monitored in this program. 1 pixel corresponds to 175 km/s for G230LB and 20 km/s at 2300 Å for G230MB.

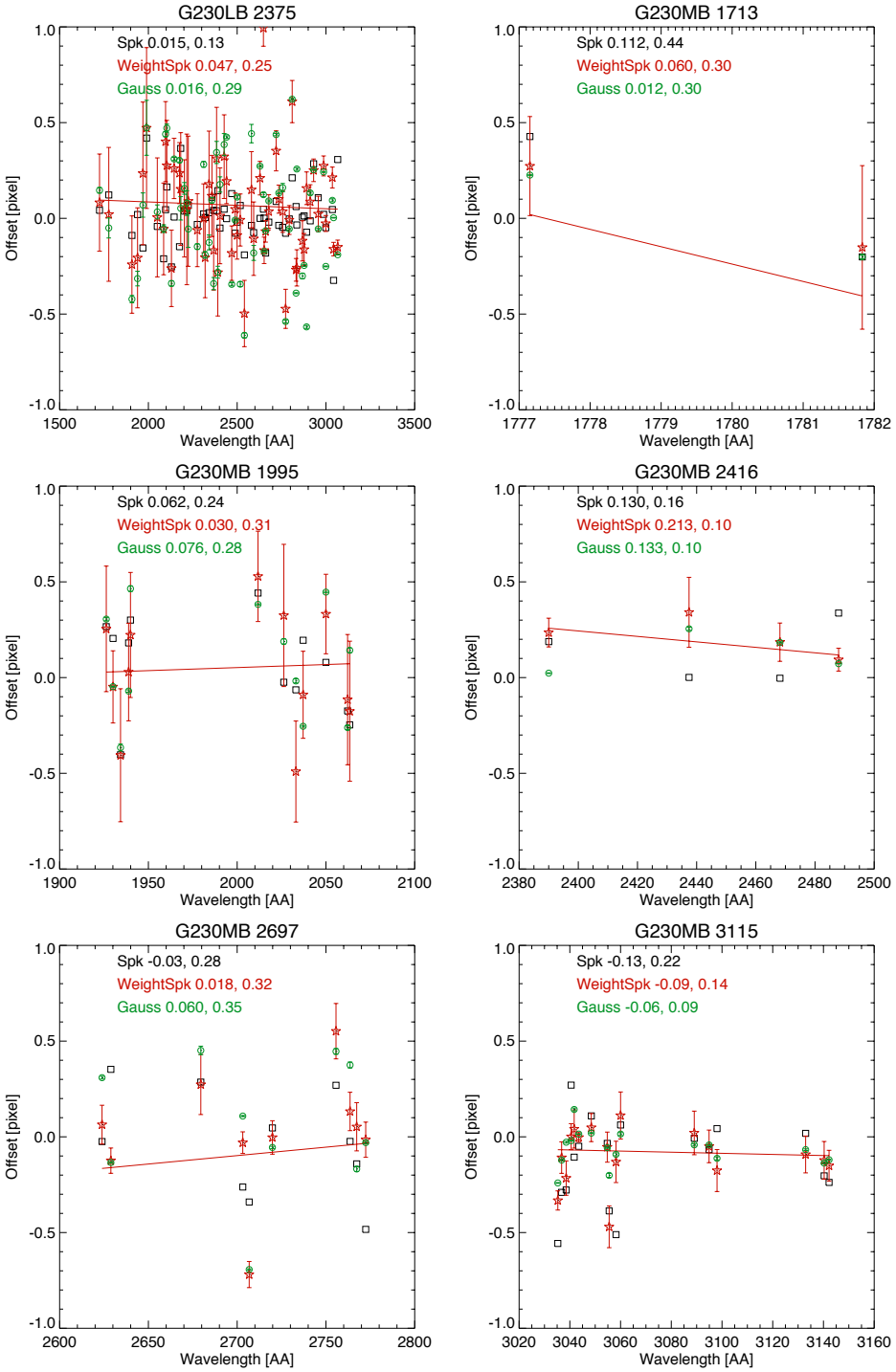

Table 2. Summary of achieved accuracy for G430L and G430M.

Grating-Cenwave	Mean Offset (pix)	Standard Deviation (pix)
G430L-4300	-0.07	0.28
G430M-3165	0.05	0.24
G430M-3680	0.01	0.27
G430M-4961	-0.06	0.09
G430M-5471	0.00	0.14

Figure 2. The achieved accuracies in Cycle 18 are consistent with those derived in Cycle 17 and fulfill the requirements for the CCD gratings and M mode combinations monitored in this program. 1 pixel corresponds to 240 km/s for the L mode and 25 km/s at 4300 Å for G430M. The 5 panels show the difference between the fitted line centroids and the corresponding laboratory wavelengths computed for all identified lamp lines. For each setting the mean and standard deviation of the latter differences were then calculated in pixel space. The green symbols show results using a Gaussian fit to the lamp emission lines. The red symbols show results using a weighted mean centroid fitting.

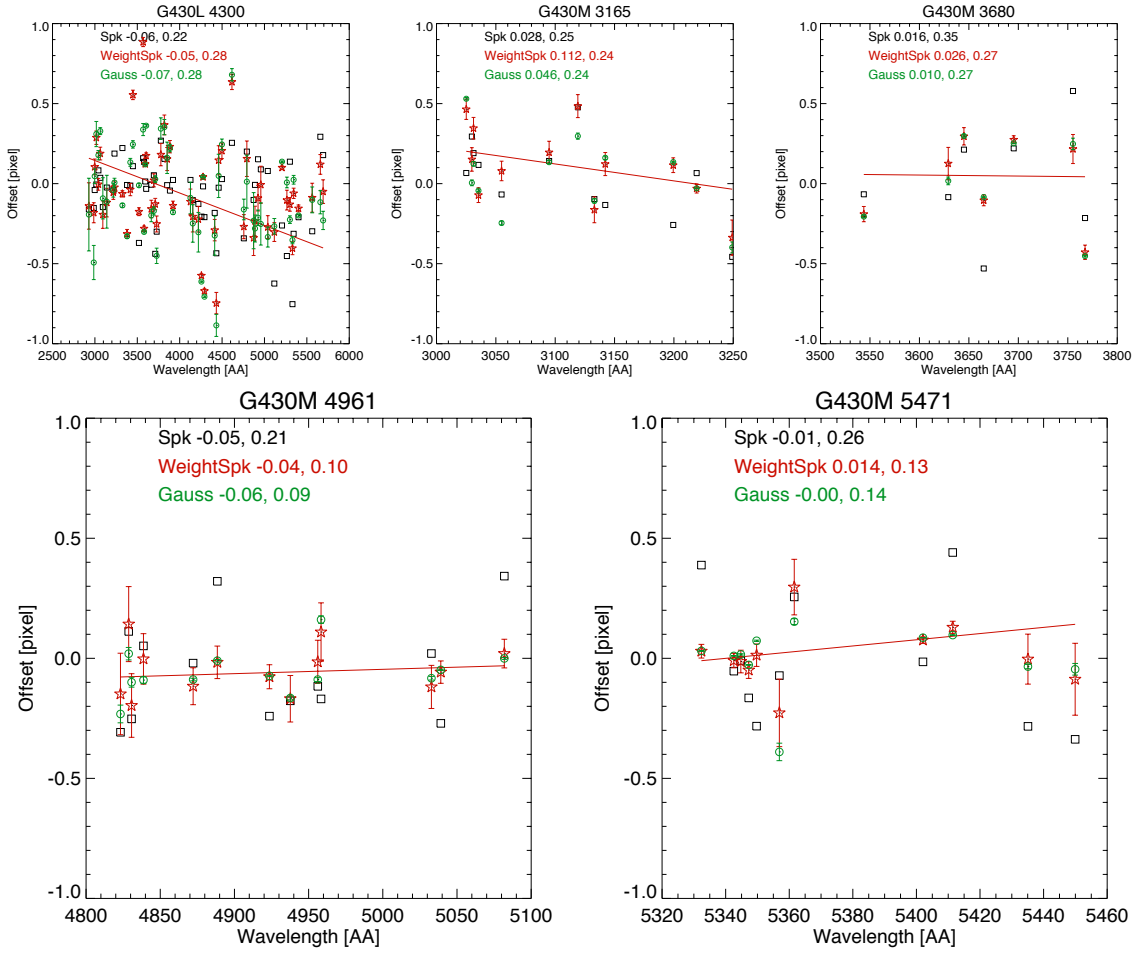

Table 3, Summary of achieved accuracy for G750L and G750M.

Grating-Cenwave	Mean Offset (pix)	Standard Deviation (pix)
G750L-7751	-0.08	0.14
G750M-5734	0.04	0.08
G750M-6768	0.01	0.04
G750M-8311	0.04	0.05
G750M-9336	-0.07	0.07

Proposal ID 12408: CCD Internal Sparse Field CTE Test (PI: Wolfe)

Analysis Lead, Others: Michael A. Wolfe and Van Dixon.

Summary of Goals

The goal was to measure and establish an accurate correction for parallel register CTE losses via internal calibration lamp observations taken through narrow slits. Revised values for the CTE correction coefficients were to be put into the ccdtab reference files if necessary. The centroid shifts of the extraction regions in the y-direction (along columns) were reviewed as they have been in the past by Goudfrooij et al. (2006).

Execution

The execution was nominal. Ten orbits were added to obtain biases in gain = 1 and 4 to create superbiases with a S/N greater than 1 using amps A and C.

Summary of Analysis

A sequence of nominally identical exposures is taken, alternating the read-out between amplifiers on opposite sides of the CCD. After correcting for gain differences in the read-out chains, the observed ratio of the fluxes seen by the two amplifiers can be fit to a simple model of constant fractional charge loss per pixel transfer. By fitting the observed flux ratio at a range of source positions along the columns, one can confirm that what is being measured is indeed a charge transfer effect. This "internal" version of the "sparse field test" is as follows. Using an on-board tungsten lamp, the image of a narrow slit is projected at five positions along the CCD columns. At each position, the alternating sequence of exposures mentioned above is taken. For each exposure, the average flux per column within a standard 7-row extraction aperture and the centroid of the image profile within those 7 rows is calculated. The alternating exposure sequence allows CTE effects to be separated from warm-up effects of the calibration lamp. A revised value for the time dependence of the CTI was determined and put into the ccdtab reference file. The centroid shifts were examined and noted that they are increasing as the CTI increases and conversely that the centroid shifts decrease in value as the effect of CTI decreases. For the very short exposure times the centroid shifts are large due to its dependence on signal levels. Short exposures have lower signal levels and smaller background. Figures 1 and 2 show the results from the charge transfer inefficiency (CTI) and centroid shift analysis. Note that the time dependence still follows a linear extrapolation of previous trends as can be seen by the new data point plotted (last data point). Note that the centroid shifts increase with decreasing signal as shown in Figure 2.

Accuracy Achieved

CTI values are accurate to within 1% for signal levels > 200 e-.

Reference Files Delivered
From this cycle's results the ccdtab reference file (* ccd.fits) was updated and a revised * ccd.fits reference file was delivered.

Relevent ISRs
None.

Continuation Plans
This program has been continued in Cycle 19 as 12769.

Supporting Details
See Figures 1 and 2.

Figure 1. CTI as a function of time. The value for the source and background can be found in the legend and is denoted as "s" for the source and as "b" for the background.

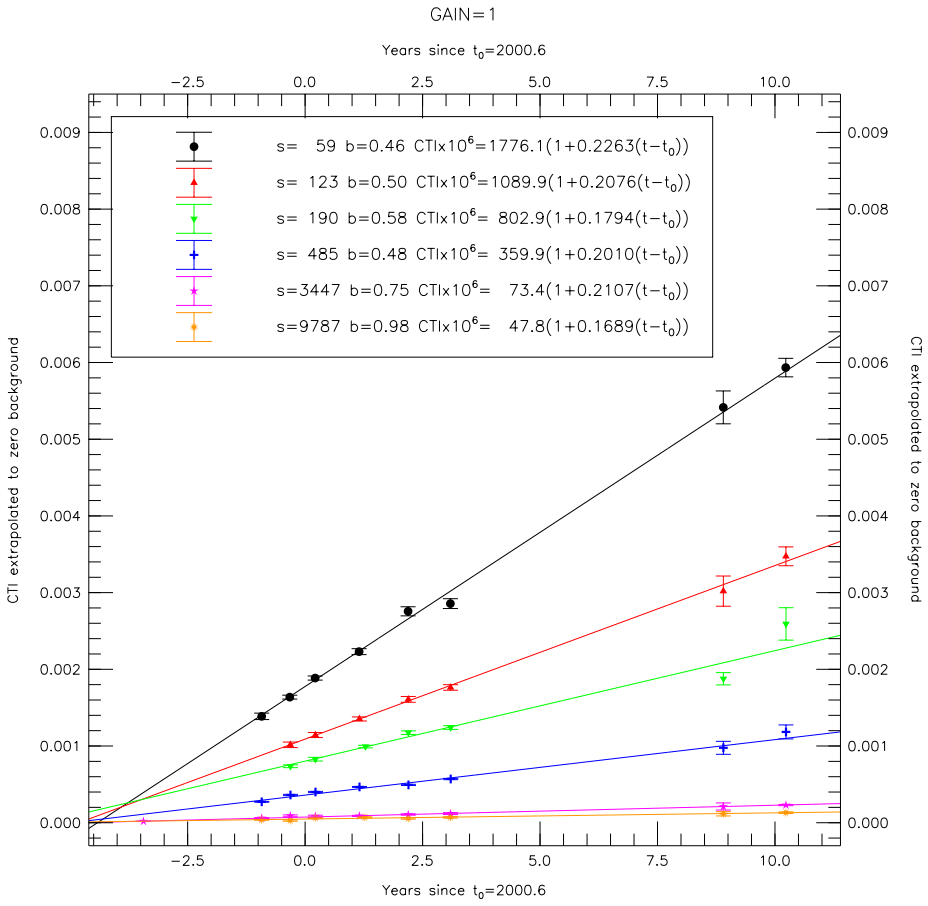

Figure 2. Centroid shift as a function of signal level.

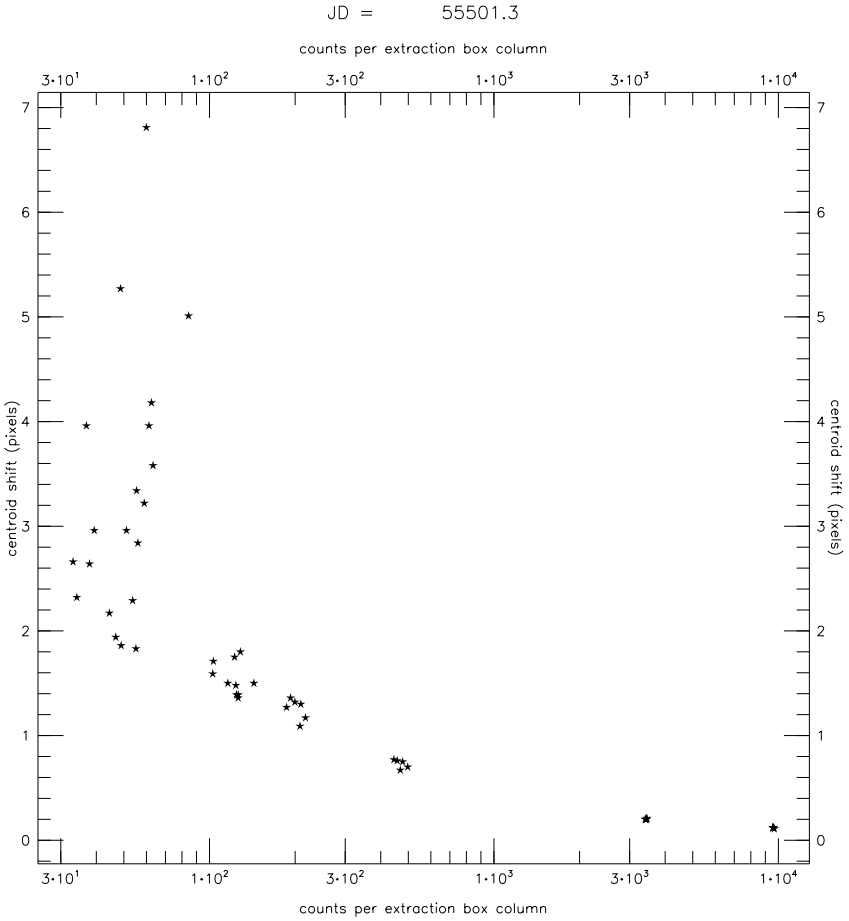

Proposal ID 12409: STIS CCD Full-Field Sensitivity Monitor C18 (PI: Van Dixon)

Analysis Lead, Others: Julia Roman-Duval

Summary of Goals
The goal was to annually monitor the STIS CCD imaging sensistivity over its whole field of view by observing a photometric standard star field in Omega Cen (NGC5139) in 50CCD. This test provided a direct transformation of the 50CCD magnitudes to the Johnson-Cousins system for red sources. These transformations were accurate to 1%. The stability of these transformations was measured to the sub-percent level. These observations also provided a check of the astrometric and PSF stability of the instrument over its full field of view.

Execution
Execution occurred as planned on 02-05-2011 between 00:41 and 02:29.

Summary of Analysis
The sensitivity of the STIS CCD is observed to decrease with time, and appears to track the linear rate measured from the STIS CCD low-dispersion sensitivity monitors. The TDS trends as a function of wavelength and time are thus obtained from spectroscopic observations, and implemented in CalSTIS for both imaging and spectroscopic STIS CCD observations. The goal of the full-field sensitivity analysis is to verify that the TDS trends derived from spectroscopic observations are applicable to imaging mode.

The star field NGC5139 is observed annually with the 50CCD (clear) filter as part of the STIS full-field sensitivity calibration program. Calibrated and geometrically corrected science files (*sx2.fits) for all STIS CCD full-field sensitivity programs up to Cycle 18 were retrieved from MAST. The dataset used in this analysis thus includes programs acquired since 2000 up to 2011 (program IDs: 8847, 8912, 9622, 10028, 11854, 12409).

All exposures, obtained with different guide stars, show astrometric offsets of ~1". We first registered all exposures with the following method. A reference exposure was chosen, taken from the earlier program 11854 (obat01050_sx2). The cross-correlation function of the reference exposure and each exposure of the data set is calculated using the IDL routine CORREL_IMAGES, and its maximum located using the IDL routine CORRMAT_ANALYZE. The location of the maximum of the cross-correlation function corresponds to the shift to be applied to the image to match its astrometry to the reference exposure.

Once all exposures are astrometrically registered to the reference exposure, a catalog of stars is identified in the reference exposure using starfinder. The input parameters of starfinder, such as minimum correlation and detection threshold, were empirically determined via a trial-and-error method. We chose a detection threshold of 10 s and a minimum correlation of 0.7. Pairs of stars closer than 0.8" were excluded from the catalog. The starfinder point source extraction algorithm requires a PSF to match with the shape of point sources. We derived the PSF directly in each

image using a pre-determined list of stars identified by eye. Each star is centroided and stacked with the IDL routine PSF_EXTRACT in order to estimate the PSF.

Our algorithm then performs aperture photometry for each star in the catalog and each STIS CCD exposure. First, the background, its standard deviation, and the FWHM of the PSF are estimated in each exposure. Second, an accurate position for each star in the catalog in each exposure is determined. Our registration algorithm is accurate to 1 pixel. Therefore, a test sub-image centered on the position of a star from the catalog, and of width 0.8" is first used to estimate the centroid position of each star in each exposure with sub-pixel accuracy. Once the centroid position is determined, a second sub-image is extracted of size 0.8" and centered on the previously calculated centroid position. Aperture photometry is performed on this sub-image, using an aperture of 5 times the FWHM of the PSF, and annulus also of radius 5 times the FWHM of the PSF, and thickness 5 pixels. The net counts are then converted to magnitudes using the exposure time and the ZMAG keyword populated by CALSTIS, and which includes a correction for the expected TDS trend.

Our algorithm thus provides a catalog of stars and their magnitudes as a function of time, covering the time period 2000-2011. For each star, the observed linear trend of magnitude vs time is fitted. Figure 1 shows the histogram of the slopes of these trends. The mean slope of the magnitude vs time trend for the STIS CCD detector is 0.2 mmag/year, with a standard deviation of 23 mmag/year (based on 108 stars). Over 15 years, this represents a change of 0.3%, lower than the quoted 1 % uncertainty. The mean weighted slope is 0.5 mmag/year (0.75% over 15 years). Figure 2 shows the time dependency of the full-field sensitivity (expressed as a slope in mmag/year) as a function of magnitude.

Studies to verify the geometric distortion solution are also in progress, and those results will be reported at a later time.

Accuracy Achieved
0.3%

Reference Files Delivered
None

Relevant ISRs
"Full-field sensitivity and its time-dependence for the STIS CCD and MAMAs", Julia Roman-Duval et al., ISR STIS 2013-02

Continuation Plans
Continued in Cycle 19 with no changes as PID 12770.

Supporting Details
None

Proposal ID 12410: Slit Wheel Repeatability (PI: Zheng)

Analysis Lead, Others: Wei Zheng, Chris Long

Summary of Goals
The purpose of this proposal is to test the repeatability of the slit wheel by taking a sequence of comparison lamp spectra with grating G230MB (2697) and the three smallest long slits (52X0.2, 52X0.1, and 52X0.05). This proposal is identical to the Cycle 12 Program 10029, and similar to activities in SMOV4 program 11383. It is anticipated that any shifts would be smaller than 0.5 pixels.

Execution
Twenty-four images were taken during a single orbit on December 02, 2010, with the Pt/Cr/Ne LINE lamp and the CCD detector and G230MB grating (centered at 2697Å). The slit wheel rotates among 52X0.2, 52X0.1, and 52X0.05. All images appear normal and show the expected count rates.

Summary of Analysis
We followed the same procedure as for previous data: 87953 (Cycle 7), 8417 (Cycle 8), 8855 (Cycle 9), 8913 (Cycle 10), 9626 (Cycle 11), 10029 (Cycle 12), 11383 (SMOV4), and 11851 (Cycle 17). We run the IRAF script *findshifts.cl* for the images taken with the same aperture, and the shifts of spectral traces are compared with that in the first image in the input list. The task *crosscor* uses the discrete Fourier transformation to calculate the X- and Y-shift between a pair of images. Since the line traces display across nearly the entire detector, it is difficult to estimate accurately the shifts along the spatial direction (AXIS2, or Y). Typical errors in the shift are around 0.15 pixel, which seems to be larger than actual values. We made slices at different parts of an image and measured the centroid position of prominent emission lines. The typical errors are approximately 0.07 pixel. We also ran the task for all images in a time sequence, regardless of slits.

The measurements of AXIS1(X) shifts in three aperture positions are shown in Figure 1, and show typical errors of 0.07 pixel. Table 1 lists the values of shift for data taken with aperture 52x0.1" The most significant shifts are between the first and second set of images, and there are slow, time-dependent trends, which are believed to be attributable to the thermal variations in the spacecraft. In previous cycles, the trends were fitted with a 3rd-order curve for each aperture and subtracted from the data. We fit them with a linear term, but without the first data point. The resultant residuals are in the order of 0.02 pixel (0.8 milli-arcsec), which are as low as those with the non-linear fits adopted for previous analysis.

Accuracy Achieved
The latest results show that the slit-wheel repeatability is on the order of 0.02 pixel. There is no sign for performance degradation. Compared to previous cycles, the recent data show a better

repeatability than seen in previous cycles (Table 2). The largest shifts are observed in Cycle 9 and SMOV4. In Cycle 18, three slits seem to exhibit different time dependence.

Reference Files Delivered
None

Relevant ISRs
None

Continuation Plans
In Cycle 19, this program has been continued as PID 12771.

Supporting Details

Table 1. Shifts in Dispersion Direction (X)

Image	Elapse Time (hour)	Shift (pixel)
obnn01gsq	0.000	0.000
obnn01guq	0.046	-0.013
obnn01gzq	0.182	-0.047
obnn01h2q	0.251	-0.069
obnn01h3q	0.268	-0.070
obnn01h5q	0.311	-0.086
obnn01h8q	0.407	-0.102
obnn01hcq	0.496	-0.142
obnn01hgq	0.615	-0.165

Figure 1. Time dependence of relative shifts. Linear fits to the data are made by excluding the first data point for each slit.

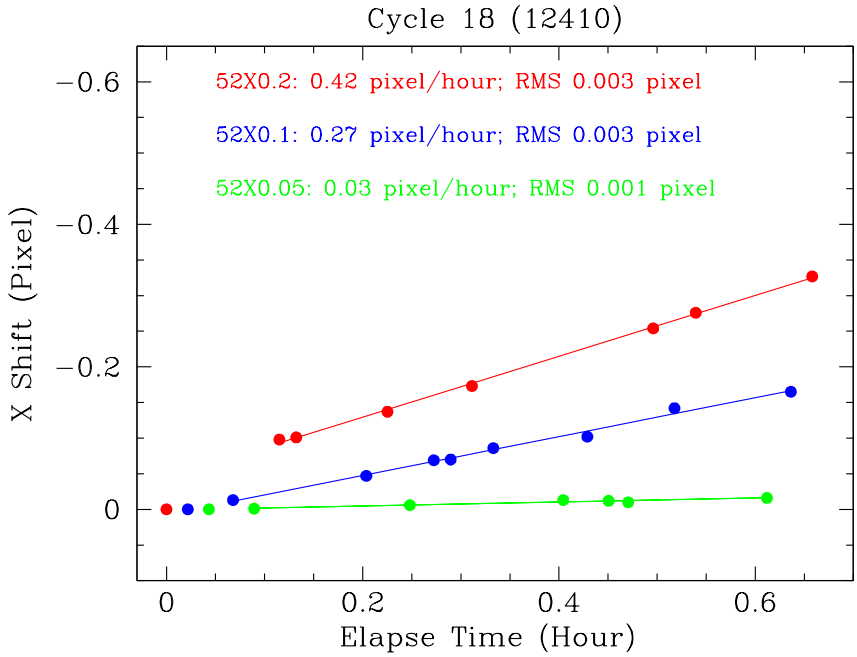

Table 2. Results of Slit-Wheel Repeatability Test (52X0.1).

Date	Cycle/Program	Drift Rate (pixel/hr)	RMS (pixel)
1999-01-25	07/7953	0.09	0.03
2000-01-12	08/8417	0.02	0.03
2001-02-08	09/8855	-0.47	0.02
2002-04-01	10/8913	-0.21	0.02
2003-03-21	11/9626	-0.01	0.02
2004-03-15	12/10029	-0.22	0.01
2009-06-03	SMOV4/11383	-0.37	0.03
2009-08-17	17/11851	-0.11	0.02
2010-12-02	18/12410	-0.27	0.00

Proposal ID 12411: STIS/CCD Spectroscopic Sensitivity Monitor for Cycle 18 (PI: Rachel Osten)

Analysis Lead: K. Azalee Bostroem

Summary of Goals
The goal is to monitor the spectroscopic sensitivity of the CCDs using both low- and medium-resolution grating setting to detect any contamination issues which might affect the spectroscopic throughput.

Execution
Visits executed on the following dates:
L1: November 22, 2010
M1: December 16, 2010
L4: April 25, 2011
L3: July 4, 2011
L2: March 14, 2011

There was a guide star failure for the L2 visit, which resulted in unusable data. This visit was replaced by the L4 visit following the approval of HOPR 67836.

Summary of Analysis
Each observation was compared to a reference spectrum to ensure that there were no anomalies. Additionally, each L mode observation was added to a plot showing the ratio of that observation to the first observation taken in that mode. Continuous piecewise linear fits were made with breaks at pre-determined points. A discontinuous breakpoint was added at 2009.5 for the G230LB. CalSTIS was modified to take a COS-like TDS reference file (with slopes and intercepts for each breakpoint) to accommodate this discontinuity.

The measured throughput for each of the three gratings is very close to what would be expected from a simple extrapolation of the trends from 2003-2004. The subsequent rate of throughput change for the G430L (-0.26%/year) and G750L (-0.17%/year) also match previous trends. The post-SM4 rate of change for the G230LB of about -0.08%/year has, however, become much flatter than the -1.44% pre-SM4 rate of decline.

Accuracy Achieved
Spectra have S/N > 50 at the wavelength of least sensitivity. Slopes are determined to an accuracy of better than 0.25% per year. After correction for time-dependent sensitivity, the relative sensitivities are determined to better than 0.3%.

Reference Files Delivered
None

Continuation Plans
This program has been continued as 12772 with no significant changes to the program.

Supporting Details
See the figures below.

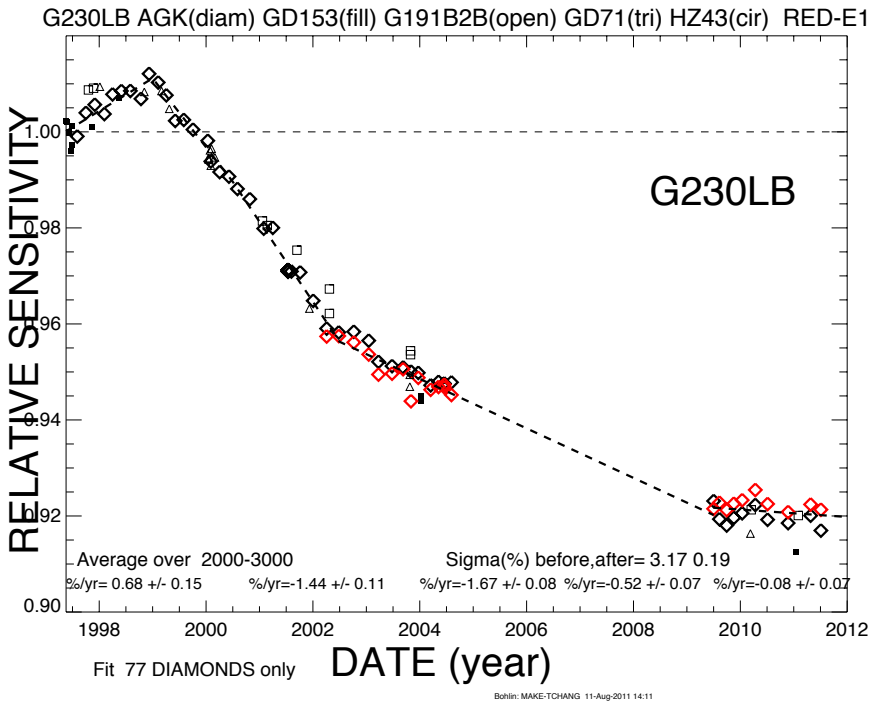

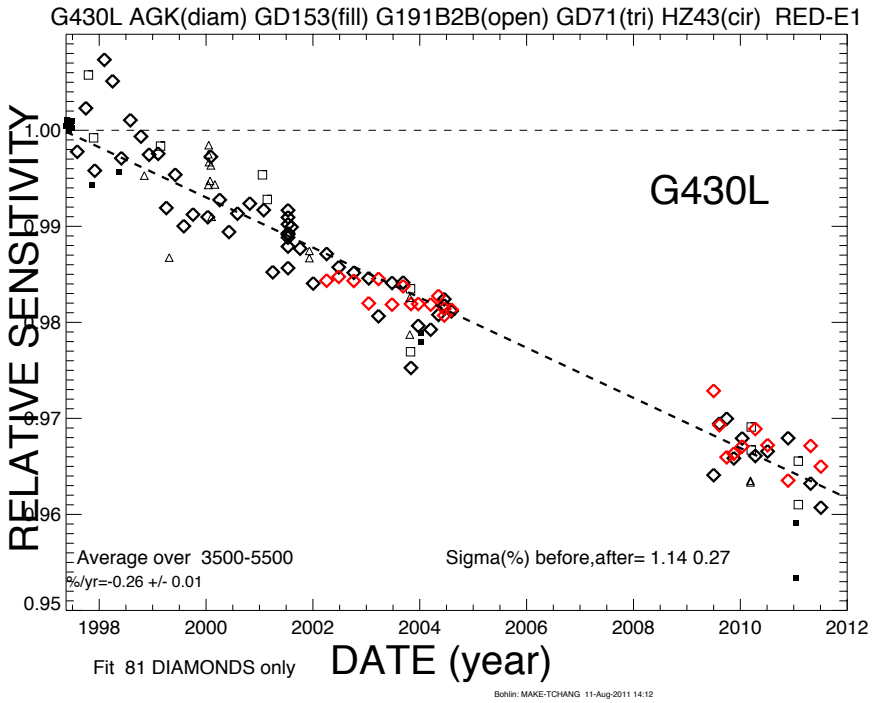
G430L AGK(diam) GD153(fill) G191B2B(open) GD71(tri) HZ43(cir) RED-E1
RELATIVE SENSITIVITY
1.00
0.99
0.98
0.97
0.96
0.95
G430L
Average over 3500-5500
Sigma(%) before,after= 1.14 0.27
%/yr=-0.26 +/- 0.01
1998
2000
2002
2004
2006
2008
2010
2012
Fit 81 DIAMONDS only
DATE (year)
Bohlin: MAKE-TCHANG 11-Aug-2011 14:12

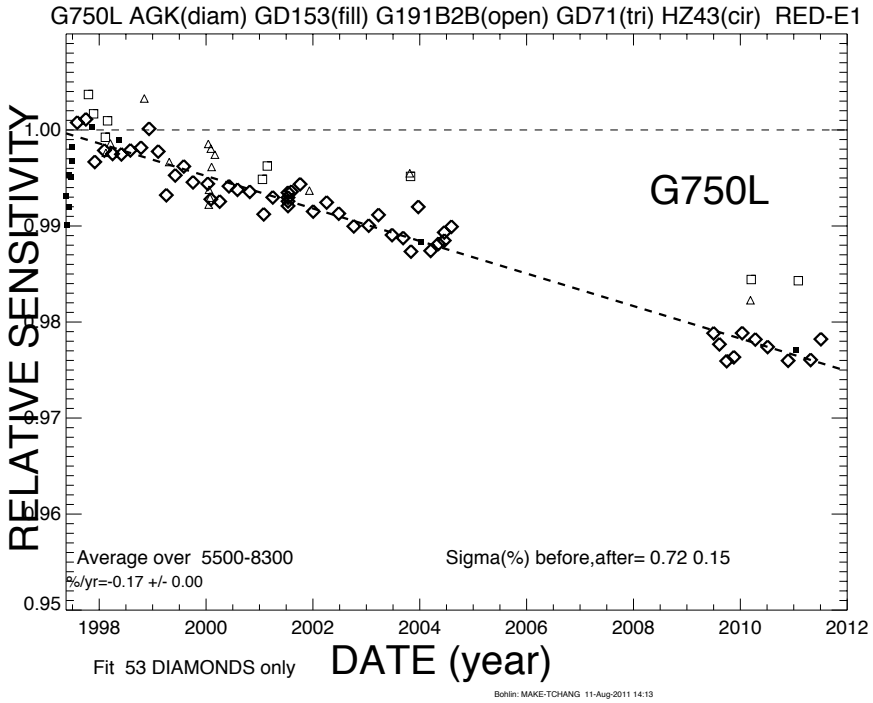
G750L AGK(diam) GD153(fill) G191B2B(open) GD71(tri) HZ43(cir) RED-E1
RELATIVE SENSITIVITY
1.00
0.99
0.98
0.97
0.96
0.95
G750L
Average over 5500-8300
Sigma(%) before,after= 0.72 0.15
%/yr=-0.17 +/- 0.00
1998
2000
2002
2004
2006
2008
2010
2012
Fit 53 DIAMONDS only
DATE (year)
Bohlin: MAKE-TCHANG 11-Aug-2011 14:13

Proposal ID 12412: MAMA Spectroscopic Dispersion Solution Monitor (PI: Pascucci)

Analysis Lead, Others: Paule Sonnentrucker

Summary of Goals
The goal is to verify the STIS MAMA dispersion solutions using internal LINE wavecal data for the E140H, E140M, E230H, E230M, G140L, G140M and G230M gratings at a total of 17 central wavelengths supported for MAMA spectroscopic observations. There were no external targets used.

Execution
Yearly monitoring executed Nov 16-18, 2010, for a total of 7 orbits, 1 visit each. The data for all grating/cenwave combinations were successfully taken. The 0.2x0.09", 0.2x0.06", 0.1x0.09 and 52x0.1 slits were used. No data loss occurred.

Summary of Analysis
The LINE lamp exposures were reduced with CalSTIS as if they were science exposures. The emission lines in the resulting x1d spectra were fitted with Gaussian profiles. The difference between the fitted line centroids and the corresponding laboratory wavelengths was computed for all identified lamp lines. For each setting the mean and standard deviation of the latter differences were then calculated.

Accuracy Achieved
The mean of the difference distribution is less than 0.1 pixel and the standard deviation is less than 0.33 pixel for all the gratings using the H mode. For the M modes, the difference distribution is less than 0.1 km/s and the standard deviation is less than 0.35 pixels. These results are consistent with those reported pre-SM4 and those reported for Cycle 17 by Pascucci et al. (2010; ISR 2011-V1).

Reference Files Delivered
No new files were delivered. There does not need to be a new delivery as the solution accuracy has not changed since Cycle 17 or since SM4.

Relevant ISRs
Not required.

Continuation Plans
The monitoring program for the MAMA dispersion solutions was carried over to Cycle 19 as Program 12773 for a total of 7 orbits, 1 visit each, as in Cycle 18. The gratings and cenwaves used in Cycle 18 were carried over to the Cycle 19 monitoring program.

Supporting Details
The figures and tables below give the mean and standard deviations derived from the monitoring data for each grating and cenwave combination.

Table 1. Summary of achieved accuracy for E140H and E230H.

Grating-Cenwave	Mean Offset (pix)	Standard Deviation (pix)
E140H-1271	0.05	0.33
E140H-1343	-0.05	0.29
E140H-1598	-0.03	0.33
E230H-1763	0.08	0.28
E230H-1963	0.03	0.32
E230H-2713	-0.01	0.28

Figure 1. The achieved accuracies in Cycle 18 are consistent with those derived in Cycle 17 and fulfill the requirements for MAMA echelle modes monitored in this program. 1 pixel corresponds to 1.3 km/. The 3 panels show the difference between the fitted line centroids and the corresponding laboratory wavelengths computed for all identified lamp lines in the E140H spectra. For each setting the mean and standard deviation of the latter differences were then calculated in velocity space. The black diamonds show results using a Gaussian fit to the lamp emission lines. The red stars show results using a weighted mean centroid fitting.

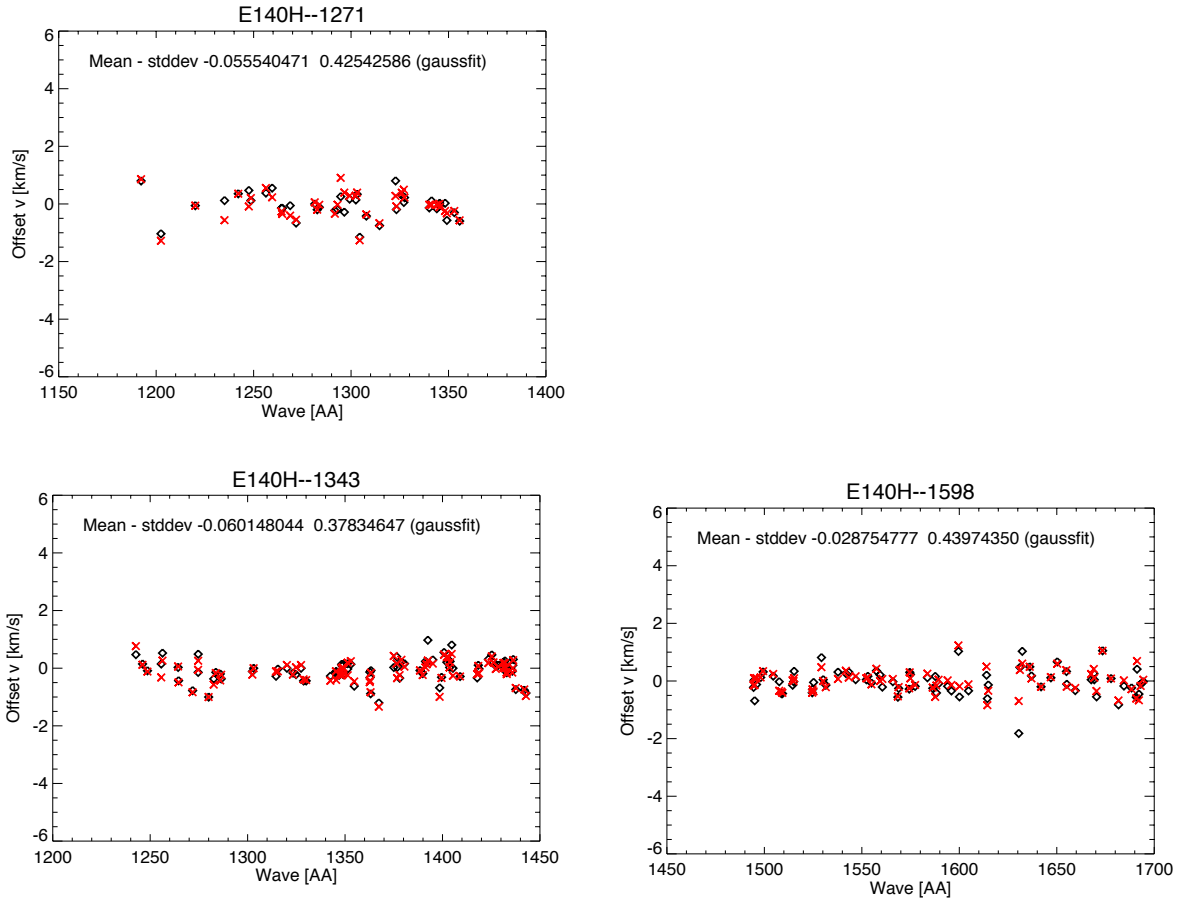

Figure 2. The 3 panels show the difference between the fitted line centroids and the corresponding laboratory wavelengths computed for all identified lamp lines in the E230H spectra. For each setting the mean and standard deviation of the latter differences were then calculated in velocity space. The black diamonds show results using a Gaussian fit to the lamp emission lines. The red stars show results using a weighted mean centroid fitting. 1 pixel corresponds to 1.3 km/s.

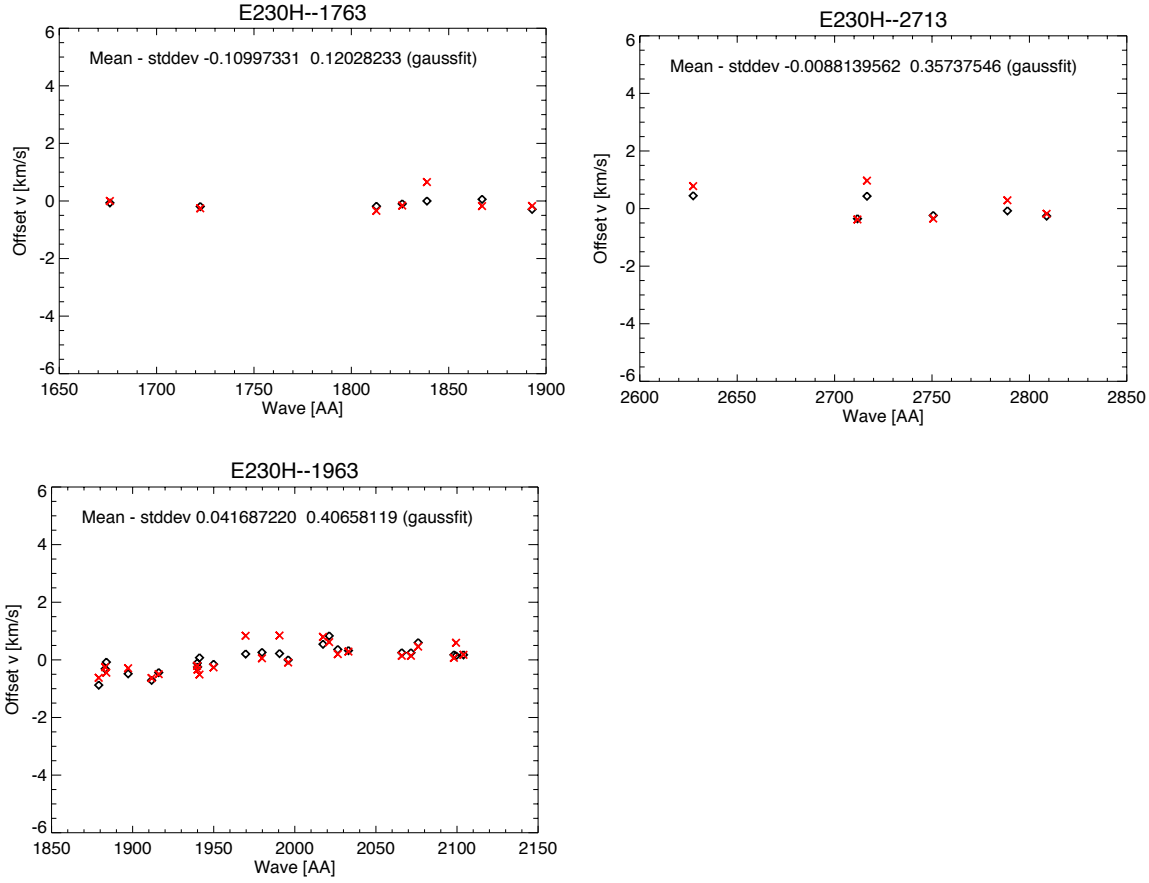

Table 2. Summary of achieved accuracy for E140M and E230M.

Grating-Cenwave	Mean Offset (pix)	Standard Deviation (pix)
E140M-1425	-0.07	0.26
E230M-1978	0.03	0.22
E230M-2415	-0.09	0.35
E230M-2561	0.05	0.33
E230M-2707	0.06	0.23

Figure 3. The achieved accuracies in Cy18 are consistent with those derived in Cy17 and fulfill the requirements for MAMA echelle modes monitored in this program. 1 pixel corresponds to 3.3 km/s. The 5 panels show the difference between the fitted line centroids and the corresponding laboratory wavelengths computed for all identified lamp lines in the E140M and E230M spectra. For each setting the mean and standard deviation of the latter differences were then calculated in velocity space. The black diamonds show results using a Gaussian fit to the lamp emission lines. The red stars show results using a weighted mean centroid fitting.

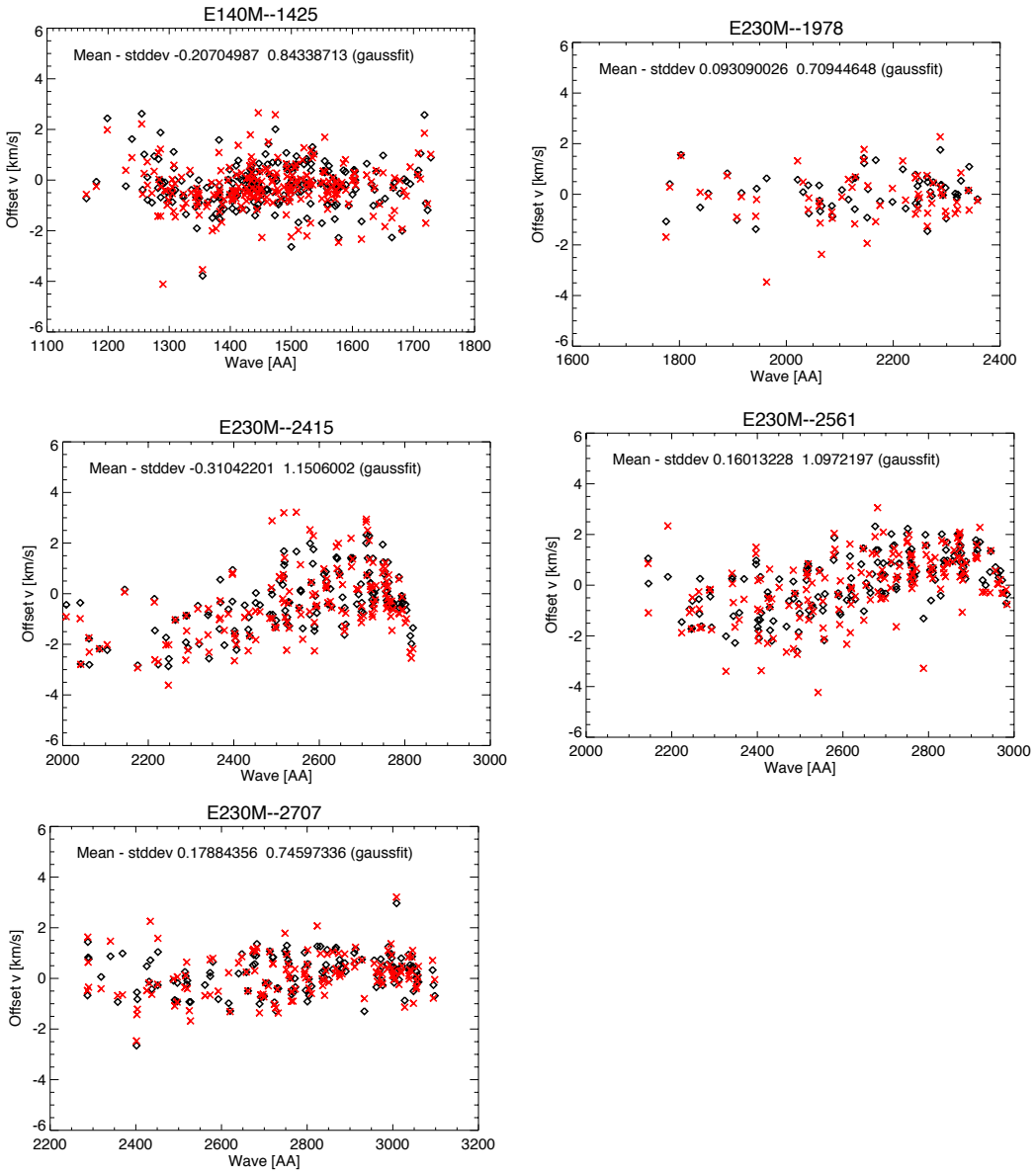

Table 3. Summary of achieved accuracy for G140L, G140M, G230L and G230M.

Grating-Cenwave	Mean Offset (pix)	Standard Deviation (pix)
G140L-1425	0.04	0.15
G230L-2376	0.02	0.08
G230M-1687	0.05	0.50
G230M-3055	0.13	0.15
G140M-1218	0.50	0.35

Figure 4. The 3 panels below show the difference between the fitted line centroids and the corresponding laboratory wavelengths computed for all identified lamp lines. For each setting the mean and standard deviation of the latter differences were then calculated in velocity space. The black diamonds show results using a Gaussian fit to the lamp emission lines. The red stars show results using a weighted mean centroid fitting. 1 pixel corresponds to 199 km/s for G230L and 16 km/s for G230M.

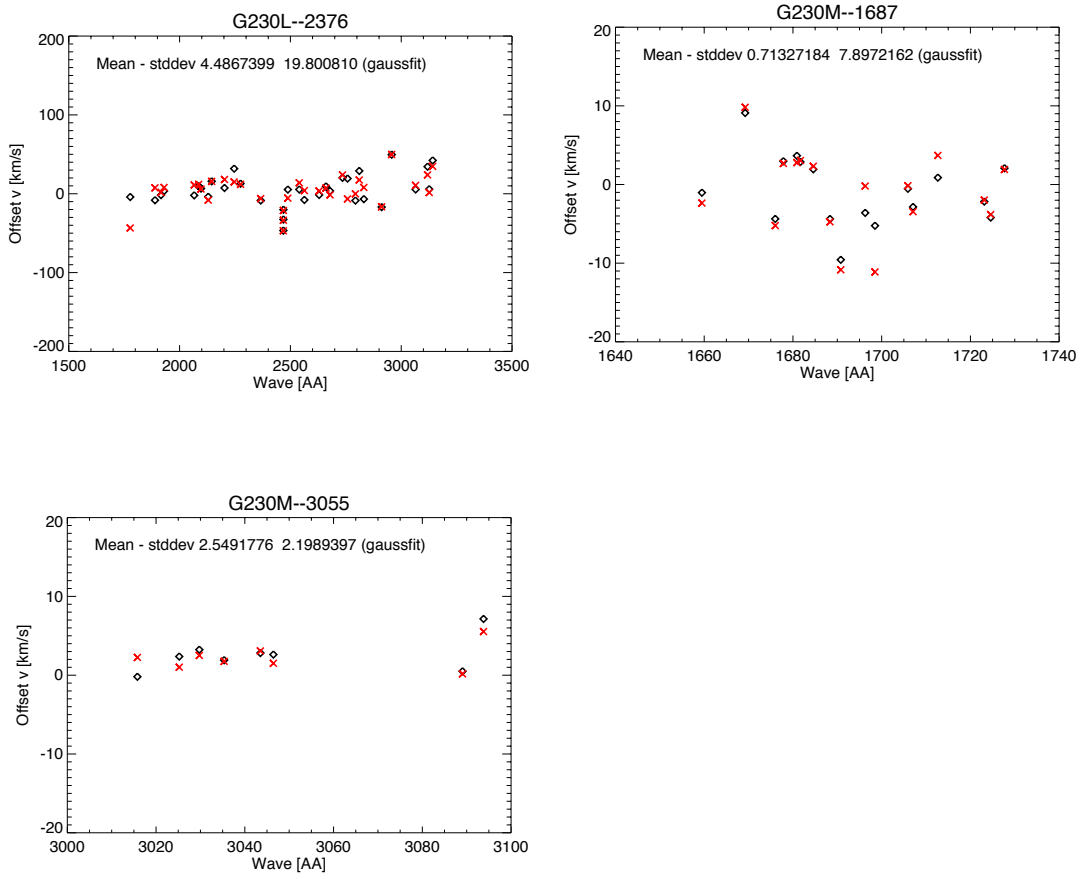

Figure 5. The 2 panels below show the difference between the fitted line centroids and the corresponding laboratory wavelengths computed for all identified lamp lines. For each setting the mean and standard deviation of the latter differences were then calculated in velocity space. The black diamonds show results using a Gaussian fit to the lamp emission lines. The red stars show results using a weighted mean centroid fitting. 1 pixel corresponds to 126 km/s for G140L and 12 km/s for G140M.

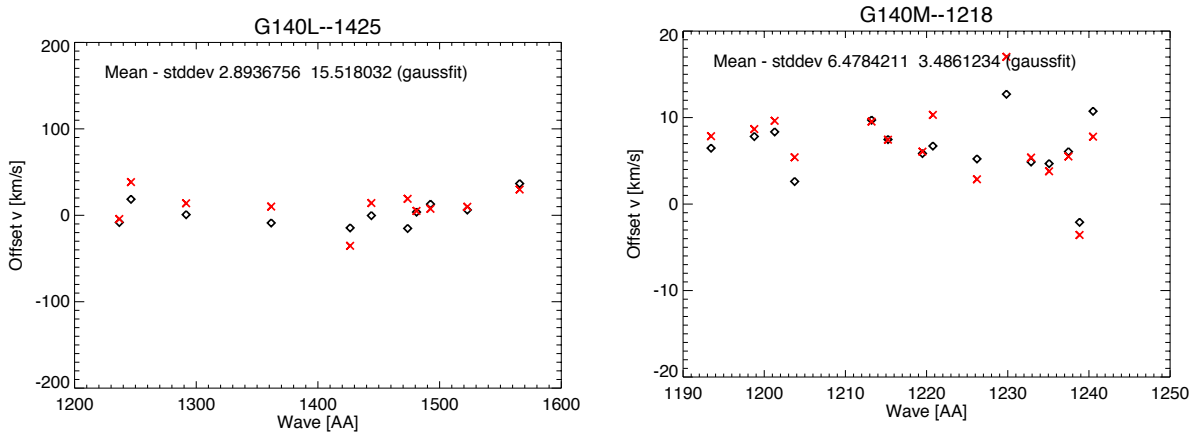

Proposal ID 12413: STIS MAMA Full-Field Sensitivity Monitor C18 (PI: Van Dixon)

Analysis Lead, Others: Julia Roman-Duval

Summary of Goals
The sensitivity of the STIS MAMAs is observed to decrease linearly with time, with a rate measured from the STIS sensitivity monitors. The TDS trends are thus obtained from spectroscopic observations, and implemented in CalSTIS for both imaging and spectroscopic STIS MAMA observations. The goal of the full-field sensitivity calibration program is to verify that the TDS trends derived from spectroscopic observations are indeed applicable to imaging mode, and correcting the decline in sensitivity in imaging mode accurately.

Execution
Execution occurred as planned on 04-16-2011 between 17:29 and 21:13.

Summary of Analysis
The globular cluster NGC6681 is observed annually as part of the STIS full-field sensitivity calibration program. The NUV images are obtained in the F25SRF2, F25QTZ, and F25CN182 filters, while the FUV images make use of the 25MAMA (clear), F25QTZ, and F25SRF2 filters. Calibrated and geometrically corrected science files (*x2d.fits) for all STIS MAMA full-field sensitivity programs up to C18 were retrieved from MAST. The data set used in this analysis thus includes programs acquired since 1997 up to 2011 (program IDs: 7080, 7132, 7720, 7788, 8422, 8425, 8858, 8918, 9623, 10032, 11856, 12413). The NUV and FUV MAMA data are analyzed independently.
All exposures, obtained with different guide stars, show astrometric offsets of ~1". We first register all exposures with the following method. A reference exposure, taken as part of program 11856, is chosen for the NUV (obav01v9q_x2d) and FUV (obav01w4q_x2d). The cross-correlation function of the reference exposure and each exposure of the data set is calculated using the IDL routine CORREL_IMAGES, and its maximum located using the IDL routine CORRMAT_ANALYZE. The location of the maximum of the cross-correlation function corresponds to the shift to be applied to the image to match its astrometry to the reference exposure.

Once all exposures are astrometrically registered to the reference exposure, a catalog of stars is identified in the reference exposure using starfinder. The input parameters of starfinder, such as minimum correlation and detection threshold, were empirically determined via a trial-and-error method. We chose a detection threshold of 10 s and a minimum correlation of 0.7. Pairs of stars closer than 0.4" were excluded from the catalog. The starfinder point source extraction algorithm requires a PSF to match the shape of point sources to. We derived the PSF directly in each image using a pre-determined list of stars identified by eye. Each star is centroided and stacked with the IDL routine PSF_EXTRACT in order to estimate the PSF.

Our algorithm then performs aperture photometry for each star in the catalog and each STIS

exposure. First, the background, its standard deviation, and the FWHM of the PSF are estimated in each exposure. The typical FWHM of the PSF is 2 pixels. Second, an accurate position for each star in the catalog in each exposure is determined. Due to geometric distortion effects, stellar positions can vary by up to 10 pixels (particularly in the FUV) between exposures, despite the removal of astrometric offsets. Therefore, a test sub-image centered on the position of a star from the catalog, and of width 0.4" is first used to estimate the centroid position of each star in each exposure. Once the centroid position is determined, a second sub-image is extracted of size 0.4" and centered on the previously calculated centroid position. This two-step centering procedure allows us to account for all the stellar flux. Aperture photometry is performed on this sub-image, using an aperture of 5 times the FWHM of the PSF, and annulus also of radius 5 times the FWHM of the PSF, and thickness 5 pixels. The net counts are then converted to magnitudes using the exposure time and the ZMAG keyword populated by CALSTIS, and which includes a correction for the expected time dependent sensitivity (TDS) trend.

Our algorithm thus provides a catalog of stars and their magnitudes as a function of time, covering the time period 1997-2011. For each star, a linear trend magnitude vs time is fitted. Figure 1 shows the histogram of the slopes of these trends. The mean slope of the magnitude vs time trend for the NUV-MAMA detector is -1.4 mmag/year, with a standard deviation of 4.9 mmag/year (based on 346 stars). Over 15 years, this represents a change of 2%. For the FUV-MAMA, the mean slope is 0.2 mmag/year (based on 46 stars), with a standard deviation of 3.9 mmag/year. This represents a change of 0.3% over 15 years. The mean weighted slope for the NUV-MAMA is 0.3 mmag/year (0.4%), and it is 0.9 mmag/year for the FUV-MAMA (1.2%). Figure 2 shows the time dependency of the full-field sensitivity (expressed as a slope in mmag/year) as a function of magnitude.

Studies to improve the geometric distortion solution are also in progress, but there results will be reported at a later time.

Accuracy Achieved
FUV-MAMA: 0.3%
NUV-MAMA: 2%

Reference Files Delivered
None

Relevant ISRs
"Full-field sensitivity and its time-dependence for the STIS CCD and MAMAs", Julia Roman-Duval et al., ISR STIS 2013-02

Continuation Plans
Continued in Cycle 19 with no changes as PID 12774.

Supporting Details

Figure 1. Example of time-dependent full-field sensitivity analysis for a star from the NUV-MAMA star catalog (left) and the FUV-MAMA star catalog (right).

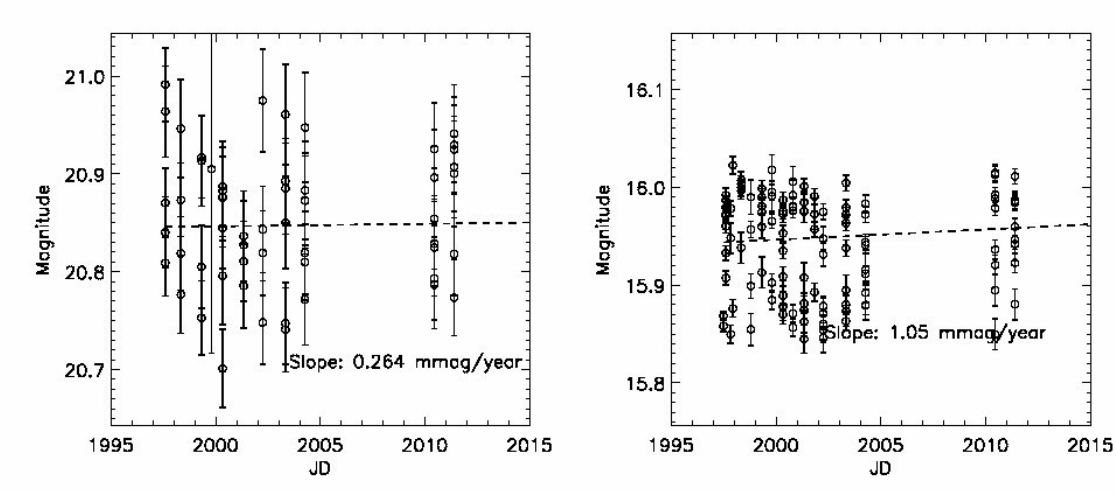

Figure 2. Histrogram of the time dependency of the full-field sensitivity for the NUV-MAMA (left) and FUV-MAMA (right).

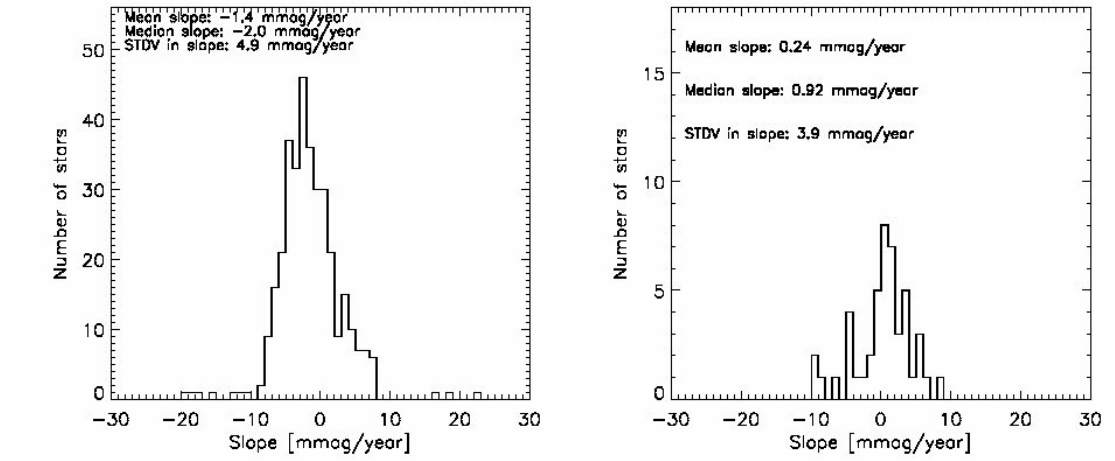

Figure 3. Slope of the full-field sensitivity time dependency as a function of magnitude in the NUV-MAMA (left) and FUV-MAMA (right) detectors.

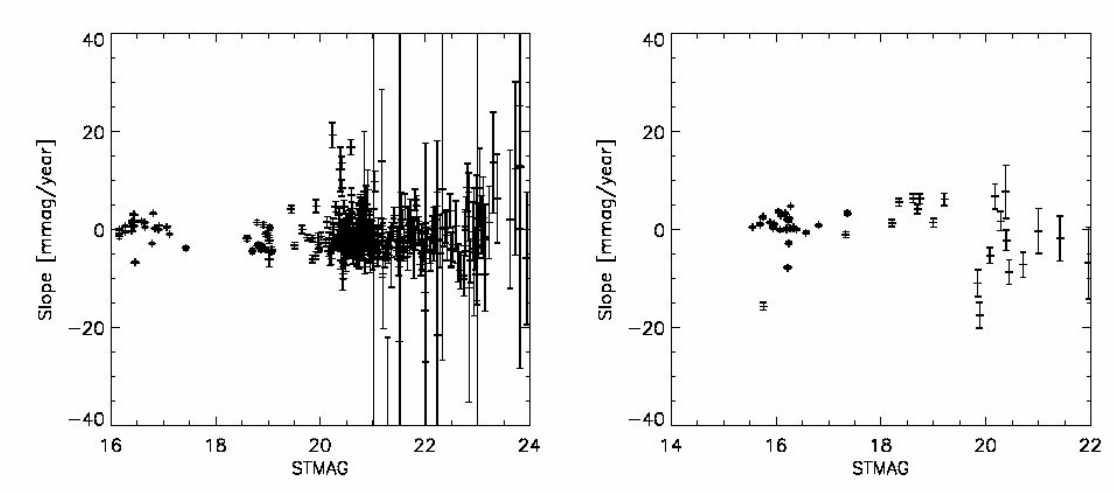

Proposal ID 12414: MAMA Spectroscopic Sensitivity and Focus Monitor Cycle 18 (PI: Rachel Osten)

Analysis Lead: K. Azalee Bostroem

Summary of Goals
The primary goal is to monitor sensitivity of each MAMA grating mode to detect any change due to contamination or other causes. The program also includes observations to monitor the STIS focus in a spectroscopic and an imaging mode, although that analysis will not be discussed here.

A secondary goal is to obtain parallel airglow spectra with COS (see COS closeout report) when possible.

Execution
Visits executed on the following dates:
E1: November 20, 2010
L1: November 20, 2010
E2: January 17, 2011
L2: March 14, 2011
E3: May 15, 2011
M1: June 13, 2011
L3: July 9, 2011
E4: August 13, 2011

There were no missed visits or anomalies.

Summary of Analysis
Each observation was compared to a reference spectrum to ensure that there were no anomalies. Additionally, each L mode and M mode observation was added to a plot that shows the ratio of the count rate measured in that observation to that of the first observation of the target done using that mode. Continuous piecewise linear fits were made with breaks at pre-determined points. A discontinuous breakpoint was added at 2009.5 for the G140L and G230L gratings. CalSTIS was modified to take a COS-like TDS reference file (with slopes and intercepts for each breakpoint) to accommodate this discontinuity. The breakpoints of G230M prior to Servicing Mission 4 were modified to best fit the data around the peak in sensitivity. A number of other small improvements were made to the fitting routine.

The G230L sensitivity appears to have been slightly increasing, at a rate of 0.17%/year, during the first two years after SM4. The scatter in the G140L results is too large to constrain the post-SM4 trend, but it appears consistent with the pre-SM4 rate of sensitivity change of about -2%/year. Results for medium resolution modes are consistent with those of the low dipsersion modes. Analysis of the echelle modes is on-going and will be reported separately.

Accuracy Achieved
Spectra have S/N > 50 at the wavelength of least sensitivity for the L modes, and at the central wavelength for the M modes. Slopes for the L modes are determined to an accuracy of better than 0.2% per year. After correction for time-dependent sensitivity, the relative sensitivities in the L modes are determined to better than 0.6%.

Reference Files Delivered
None

Continuation Plans:
This program has been continued as 12775 with no significant changes to the program.

Supporting Details
See figures below.

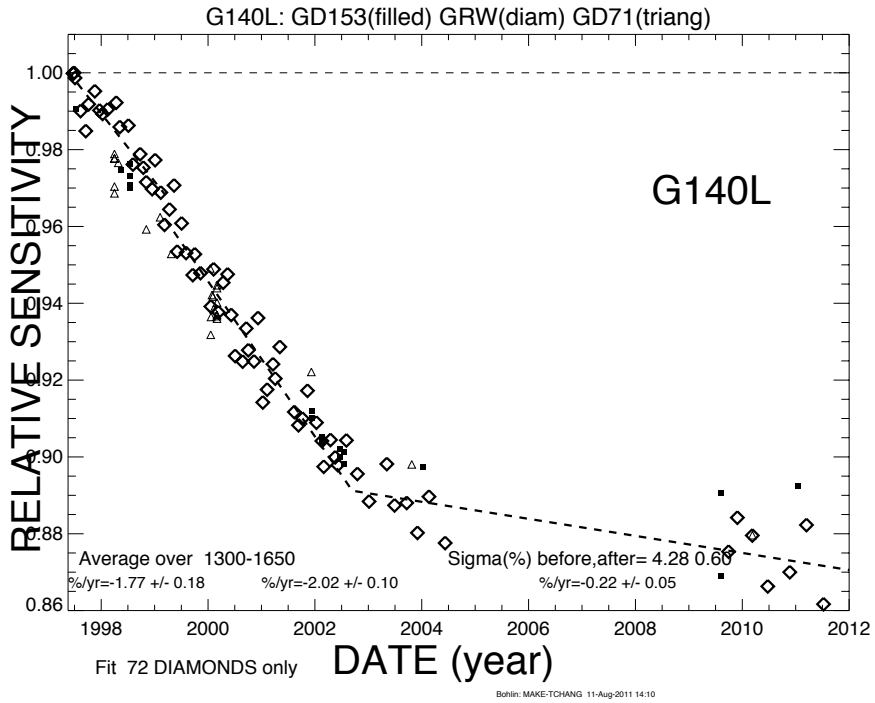

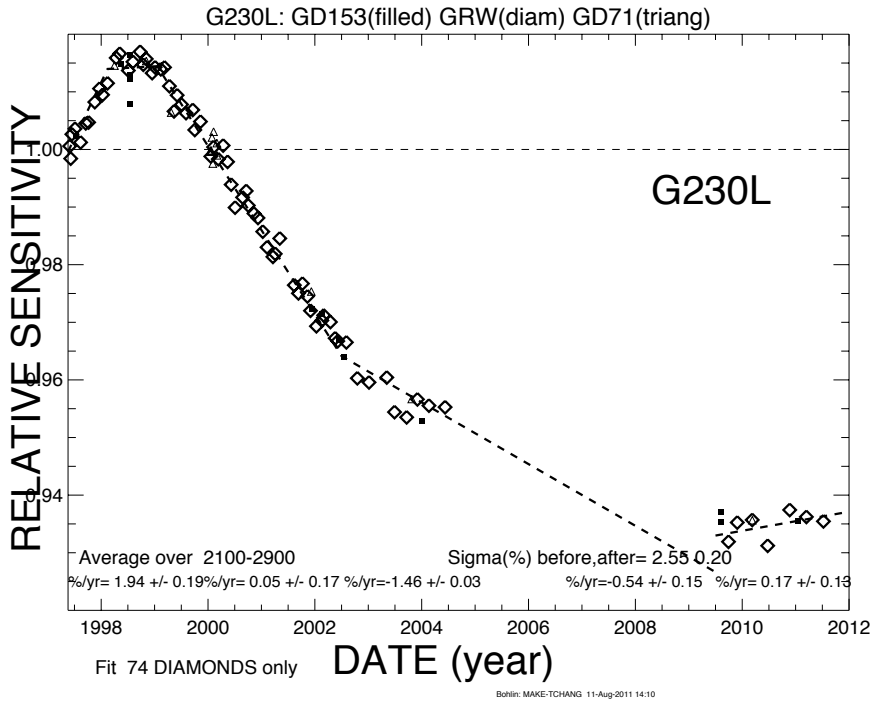
G230L: GD153(filled) GRW(diam) GD71(triang)
RELATIVE SENSITIVITY
1.00
0.98
0.96
0.94
G230L
Average over 2100-2900
Sigma(%) before,after= 2.55 0.20
%/yr= 1.94 +/- 0.19%/yr= 0.05 +/- 0.17 %/yr=-1.46 +/- 0.03
%/yr=-0.54 +/- 0.15 %/yr= 0.17 +/- 0.13
1998
2000
2002
2004
2006
2008
2010
2012
Fit 74 DIAMONDS only
DATE (year)
Bohlin: MAKE-TCHANG 11-Aug-2011 14:10

Proposal ID 12415: MAMA Dark Monitor (PI: Wei Zheng)

Analysis Lead, Others: Colin Cox

Summary of Goals
The goal is to monitor the dark detector count rate in both STIS MAMS detectors and look for any evidence of changes indicative of problems.

Execution
Two 1300-second exposures are taken bi-weekly at extreme ends of a SAA free interval to monitor both long and short term effects. All visits completed except one missed during a September 2011 HST problem.

Summary of Analysis
Figure 1 shows the NUV dark rate as a function of time from SM4 through the end of Cycle 18. For the NUV MAMA detailed analysis was performed to model the dark rate. Dark images and tables used to apply the results of the model were delivered. The dark rates can be modeled with rapid declines on time scales of several weeks plus a long-term variation in time scale that is over three years. The NUV dark rate increases after the detector has been unpowered for a significant amount of time, but then resumes its decline after its return to operations. Currently, the typical rate is about 3000 counts per second over the whole detector, or $3x10^{-3}$ count/sec/pixel. The dark rate is dependent on the detector temperature, and the newly derived parameters are different from those prior to August 2004.

The FUV dark observations are shown in Figure 2. The points shown as blue circles are the mean rates across the whole detector. Within this group there are values near 10^{-5} counts/pixel/sec and others near 10^{-4} counts/pixel/sec. These correspond to the count rates at initial turn on and at the end of the SAA-free period, at least six hours later. The red circles show the mean rate in the part of the detector with the largest dark rate, (the glow region). This follows the same trends as the average detector rate, but at about three times the level. There is no discernible long term pattern, but between October and November 2010 STIS was not operable because of an HST operational problem. After the break the rates returned at a level higher by about 50%. This has not noticeably declined since then.

Accuracy Achieved
5% to 10% in the modeled dark rate.

Reference Files Delivered
tcl1742bo_drk.fits. Dec 21 2009
tcl1742co_tdc.fits Dec 21 2009
v2a1955fo_tdc.fits Jan 25 2011

Relevant ISRs
"Dark Rate of the STIS NUV detector", Wei Zheng et al., ISR STIS 2011-03.

Continuation Plans
This program has been continued in Cycle 19 as proposal 12776, PI: Colin Cox

Supporting Details
See Figures 1 and 2 on the next page.

Figure 1. The observed STIS NUV detector dark rate as a function of time between SM4 and the end of Cycle 18.

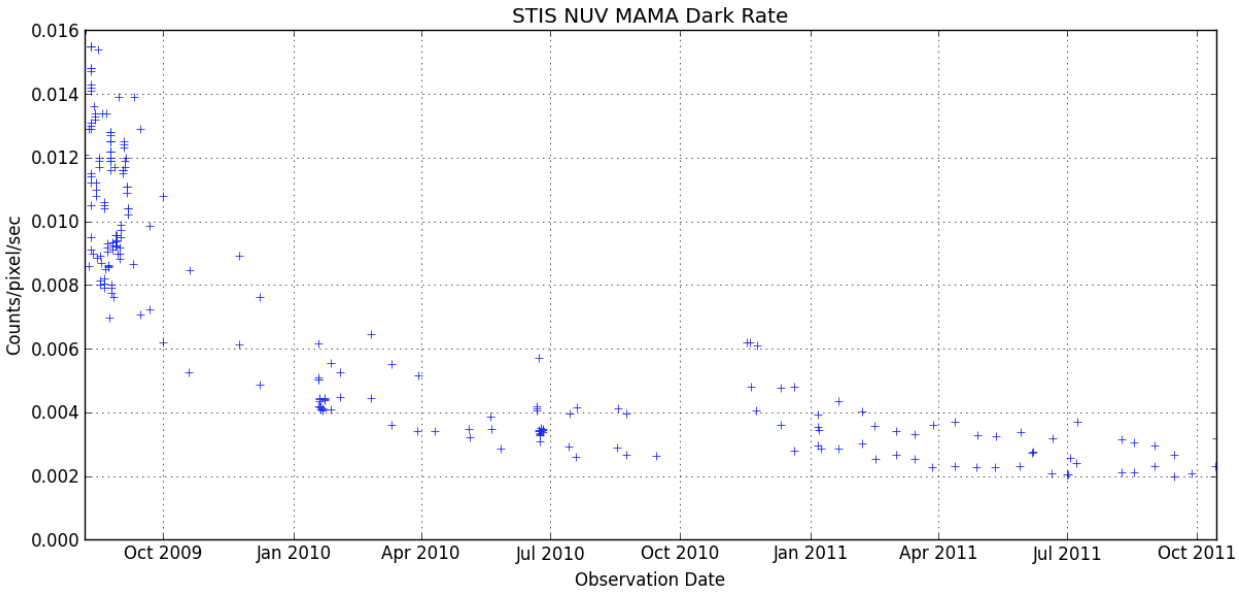

Figure 2. The observed STIS FUV dark rate as a function of time between July 2009 and August 2012 is shown. The blue symbols show the average rate over the whole detector, while the red circles show the rate in the bright "glow" region.

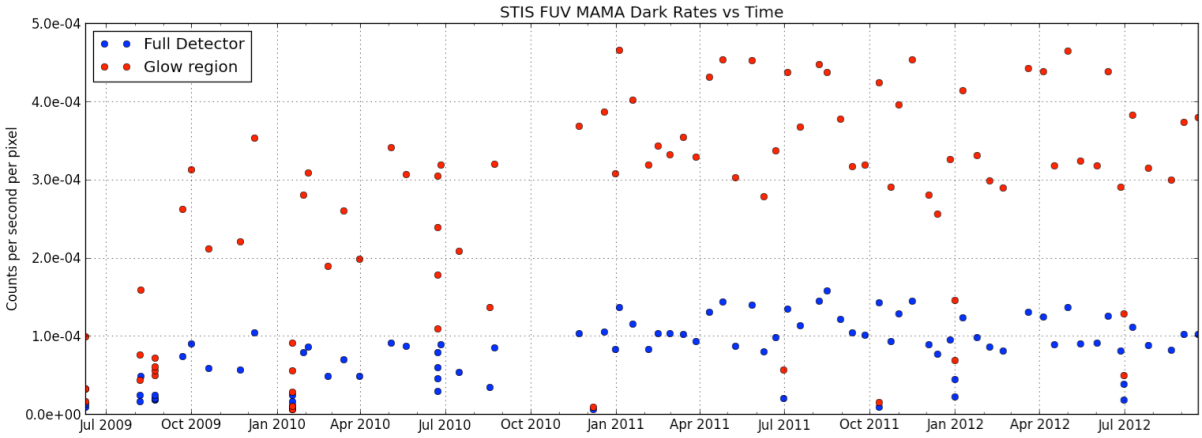

Proposal ID 12416: STIS MAMA Fold Distribution (PI: Thomas Wheeler)

Analysis Lead, Others: Thomas Wheeler, backup: Chris Long

Summary of Goals
The performance of MAMA microchannel plates can be monitored using a MAMA fold analysis procedure that provides a measurement of the distribution of charge cloud sizes incident upon the anode giving some measure of change in the pulse-height distribution of the MCP and, therefore, MCP gain. The goal of 12416 is to continue monitoring the two STIS MAMA detectors and comparing the results with previous test results to detect trends or anomalous behavior.

Execution
This proposal successfully executed on May 1, 2011

Summary of Analysis
The engineering telemetry data was examined (voltages, currents, temperatures, relay positions, and status) for agreement with predicted values and previous ground and on-orbit test data. The MAMA engineering telemetry event counter was used to construct a histogram of the number of counts for each fold. The results for each detector are compared and combined with previous test results. Post test, a dark exposure was taken where the counters were cycled and were plotted in a histogram and compared with earlier results.

No anomalous behavior was detected for either MAMA. The NUV MAMA does exhibit a known high dark count rate caused by widow phosphorescence that has been decreasing since SMOV4. Results are sent to V. Argabright of Ball Aerospace for review and comments.

Below are the FUV and NUV fold histograms followed by the post-test dark count histograms.

Accuracy Achieved
Position of the peak in the fold distribution can be measured to about 5% accuracy from this procedure.

Reference Files Delivered
N/A

Relevant ISRs
No ISRs will be published.

Continuation Plans
This monitoring program will continue in Cycle 20. The program ID is 12778.

Supporting Details
See figures on the following pages.

Figure 1. FUV MAMA Fold Histogram

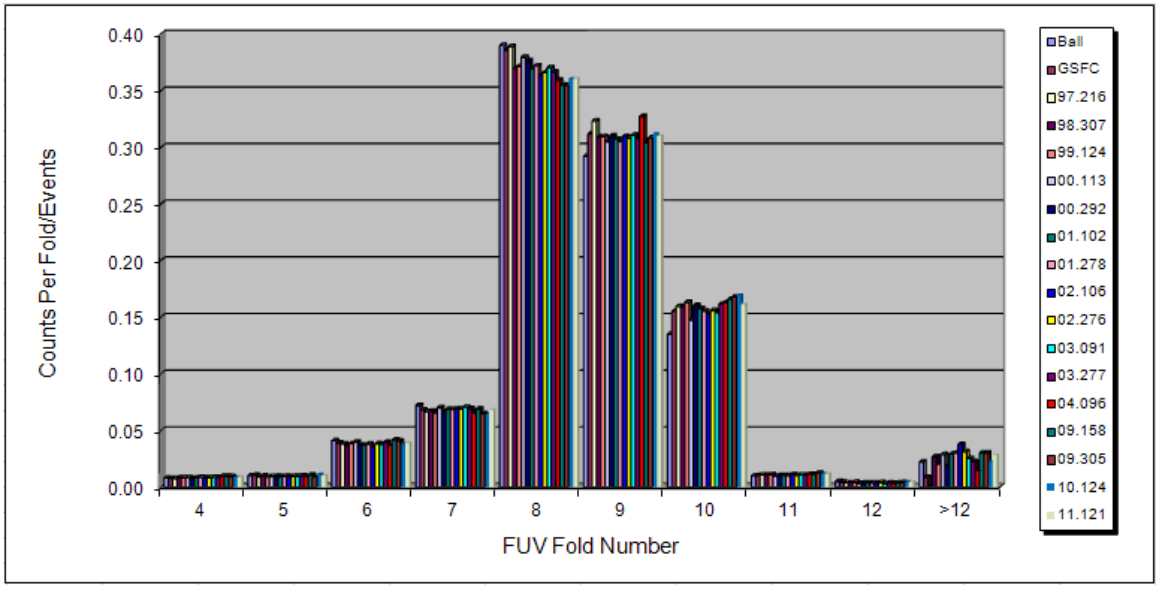

Figure 2. FUV MAMA Post-Test Dark Count Rate

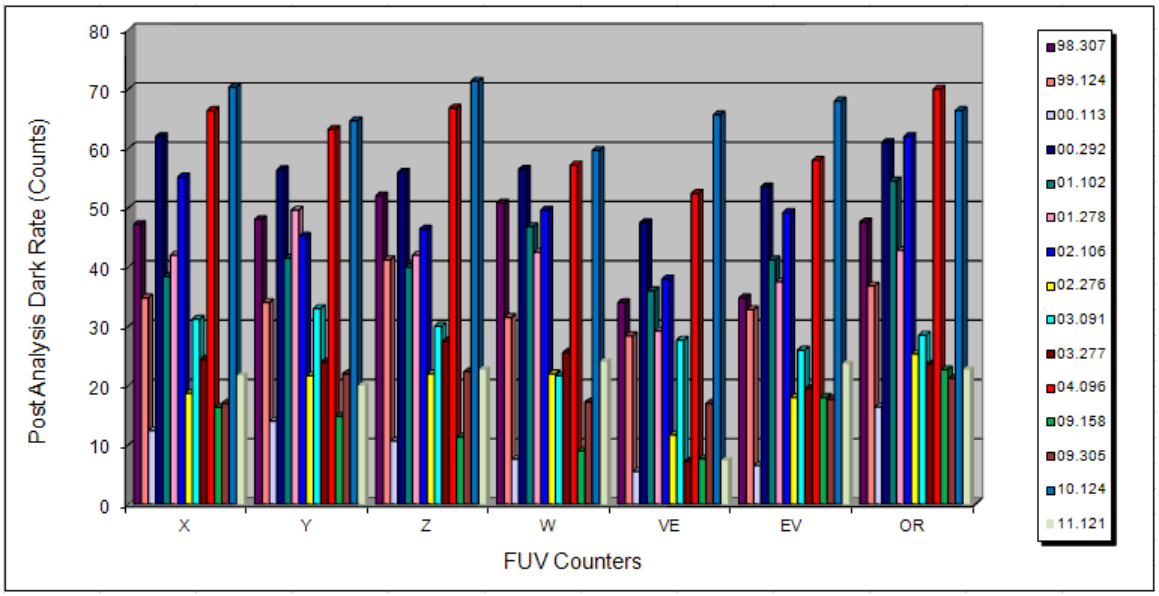

Figure 3. NUV MAMA Fold Histogram

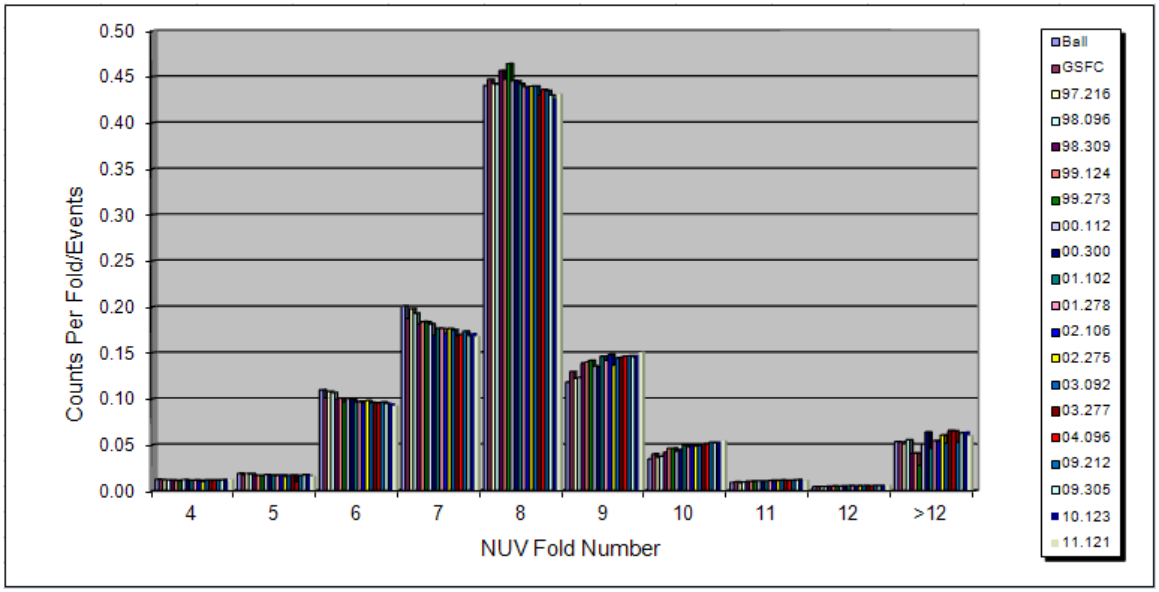

Figure 4. NUV MAMA Post-Test Dark Count Rate

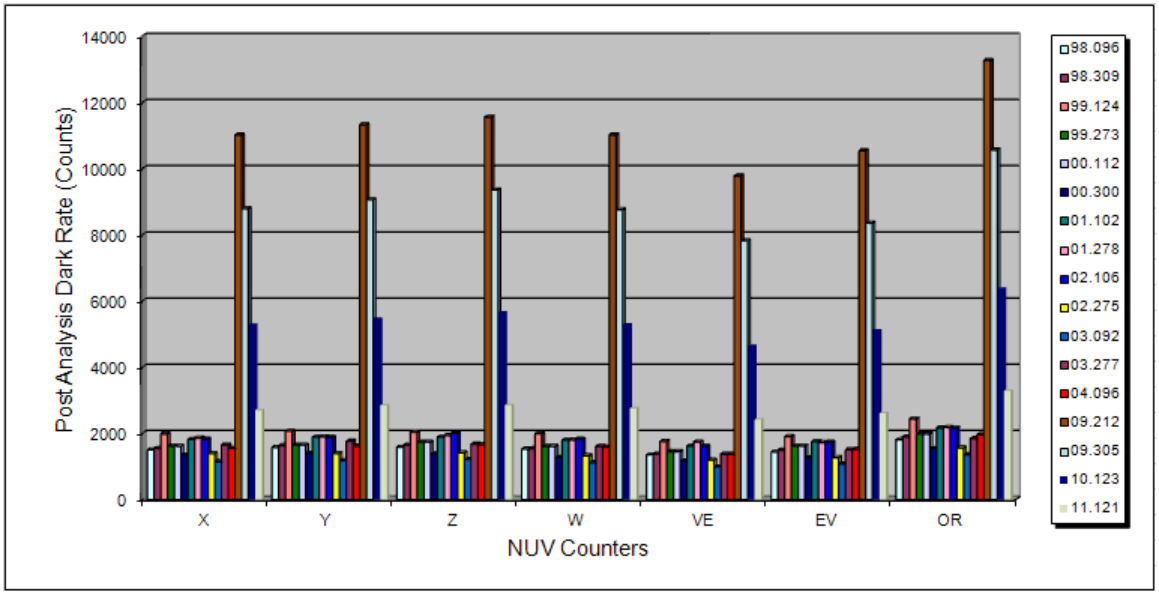

Proposal ID 12417: MAMA FUV Flats (PI: Wolfe)

Analysis Lead, Others: Michael A. Wolfe

Summary of Goals
The goal was to determine the pixel-to-pixel response (p-flat) of the FUV detector, applicable to all FUV modes. Results will be compared with the response derived in previous cycles, to look for changes. If warranted, the data will be co-added with data from previous cycles to improve S/N in the reference file.

Execution
The execution of the program was nominal.

Summary of Analysis
Due to limited resources, analysis was limited to inspection of the individual flat-field images to determine if the structure and the count rate in each flat were nominal. Each flat image was visually inspected and the count rates were calculated in the center of each image. This revealed no structural anomalies., The count rate in each flat was calculated by taking the mean count rate in a 100x100 pixel area in the center of the flat; observed rates were determined to be sufficient, *i.e.,* there was no other combination of gratings and central wavelengths that would have allowed a larger count rate without exceeding bright object protection limits (see Shaw, Kaiser, and Ferguson 1998). The count rate for each observation can be found in Table 1.

Accuracy Achieved
The signal-to-noise per pixel is S/N = 52.96 +/- 0.0189 after combining all 11 exposures and calculating Poisson statistics over an area of 2500 pixels (50x50 pixels). This translates to an accuracy level of 1.89% (1 sigma). For individual exposures the signal-to-noise per pixel is S/N ≈ 15.97 +/- 0.0057 and the accuracy level is 0.57% (1 sigma). We established that there was no change in the structure of the flats.

Reference Files Delivered
None.

Relevent ISRs
None.

Continuation Plans
This program has continued in Cycle 19 as program 12777.

Supporting Details
See Table 1 on the next page.

Table 1. FUV Flat Count Rate (e-/s)

Rootname	Mean Count Rate in Specified Area (e-/s)
obnp01d8q	224292
obnp02dfq	239578
obnp03mfq	231990
obnp04jlq	222865
obnp05brq	216353
obnp06eaq	213912
obnp07raq	220275
obnp08csq	212028
obnp09cmq	214402
obnp10neq	206259
obnp11g0q	209206

Proposal ID 12429: STIS MAMA Recovery after Anomalous Shutdown (PI: Thomas Wheeler)

Analysis Lead, Others: Thomas Wheeler, backup: Chris Long, Alan Welty,

Summary of Goals
The goal is verify that the detector has not been damaged and is returned to science operations in safe and orderly manner after an anomalous HV shutdown. The recovery procedure consists of three separate tests (i.e. visits) to check the MAMA's health; they must be completed successfully and in order. Diagnostic time-tag images are obtained in tests 2 and 3. This proposal executes the same steps as Cycle 17 proposal 11864. The tests are:

1. Signal processing electronics check
2. Slow, intermediate voltage high-voltage ramp-up where the MCP HV MCP HV is slow-ramped to a voltage 300V below nominal
3. Ramp-up to full operating voltage.

This is followed by a fold analysis test. See STIS ISR 98-02R.

Execution
This is a contingency proposal only used in the event of an anomalous HV shutdown. It was not necessary to execute any of these visits during this cycle.

Summary of Analysis
The analysis is divided into three parts with each part supporting one of the defined tests describe above:

1. Signal processing electronics check. This is the first test of three to recovering a MAMA detector. The purpose is to check out the low voltage power supply and the signal processing chain. An Excel workbook all of the engineering telemetry mnemonics to be examined (voltage, currents, temperatures), the expected values, and the allowable tolerances will be created. A pass/fail column will be defined. Engineering data will be placed into the workbook and compared to expected values.

Next the charge amplifier threshold voltage will be reduced from its nominal value of 0.48 volts to 0.28 volts. This will allow electronic noise to pass through the charge amplifiers and generate events. The number of events per seconds will be compared to the expected number +/- a tolerance for a given MAMA tube temperature.

The pass criteria for this test are that engineering telemetry and the expected number of OR counts are within expected values.

The pass criteria for this test are that engineering telemetry is within expected values and no hot spots or unusual features are observed in the science images.

2. The first high voltage ramp-up will be to an intermediate MCP voltage of 300V below the nominal MCP voltage with plateaus. This voltage ramp-up is to condition the high voltage power supply and the MCP. All the engineering telemetry described in step one will be re-examined along with the MCP voltage and current. The MCP voltage +/- a tolerance should be the commanded voltage and the MCP current +/- a tolerance should fit the MCP current model. The pass criteria for this test are that the engineering telemetry is within expected values and no hot spots or unusual features are observed in the diagnostic science images.

3. The final high voltage ramp-up is to the nominal MCP voltage with voltage plateaus followed by a fold distribution test. This is the last high voltage ramp-up to condition the high voltage power supply and the MCP. All the engineering telemetry described in step one will be re-examined along with the MCP voltage and current. The MCP voltage +/- a tolerance should be the commanded voltage and the MCP current +/- a tolerance should fit the MCP current model.

When the MCP successfully reaches the nominal value, a fold test will be performed. This data will be processed using the "standard fold test analysis tool". The results will be compared to previous fold test results.

The pass criteria for this test are that the engineering telemetry is within tolerance, no hot spots or unusual features are observed in the diagnostic science images and the fold test yields the expected results and show no significant degradation when compared to previous fold tests.

Accuracy Achieved
N/A

Reference Files Delivered
N/A

Relevant ISRs
If an anomalous HV shutdown were to occur, this would be reported in a TIR.

Continuation Plans
This is a contingency proposal. A duplicate proposal was created for Cycle 19. The proposal ID is 12779.

Supporting Details
All relevant turn-on telemetry data will be entered into an Excel workbook similar to that used in SMOV4.

Proposal ID 12418: New COS Flux Standard (PI: Derck Massa)

Analysis Lead, Others: Derck Massa, Ralph Bohlin, Pierre Chayer

Summary of Goals
DB white dwarfs (WDs) are ideal stars for FUV flux calibration. Unlike the DA WDs which are typically used, DBs do not have strong photospheric Lyman absorption lines and their flatter SEDs provide a more uniform S/N when recorded by the COS UV detectors. This proposal requests the observations needed to derive a calibration-quality model for the DB WD star WD0308-566.

Execution
Complete STIS low resolution spectra were obtained as expected.

Summary of Analysis
Ralph Bohlin reduced the STIS spectra to produce a low noise, well calibrated spectrum spanning the wavelength range from 1140 to 9000 Å. These data were passed on to Pierre Chayer who, along with his colleagues in Montreal, produced a model atmosphere for the star. This project was then determined to be of low priority, and additional work was deferred. However, the initial model has proved very useful for subsequent COS flux calibration work.

Accuracy Achieved
A S/N of 50/1 or better over 10-Å bins was achieved, as is required if the star is to become a fundamental calibration source and accurately modeled.

Reference Files Delivered
None

Relevant ISRs
None

Continuation Plans
No directly linked Cycle 20 programs have been submitted, but the WD0308-566 has proven to be a useful calibration target and additional observations of it have been obtained in other programs.

Supporting Details
See Figure 1 illustrating the spectrum of WD0308-566 on the next page.

Figure 1. Showing a portion of the Bohlin reduction of the STIS spectra of WD0308-566. It also shows why DBs are desirable UV calibration sources. There is a lack of lines in the UV, but several in the optical. As a result, there are ample optical lines to constrain a model atmosphere of the object and very few UV lines to interfere with its use a calibration sources.

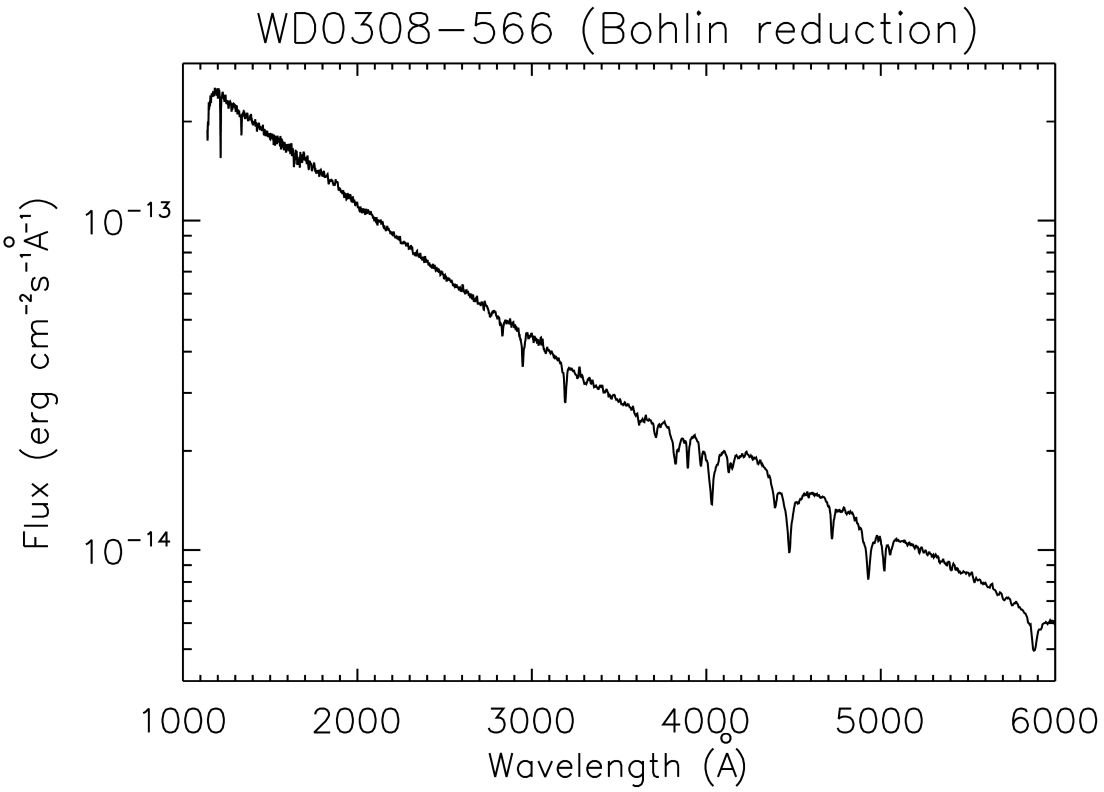

4. Change History for STIS ISR 2013-03

Version 1: 20 November 2013 - Original Document

5. References

Ferguson, H., Clampin, M. & Argabright, V. 1998, "Cycle-7 MAMA Pulse height distribution stability: Fold Analysis Measurement", ISR STIS 98-02R.

Pascucci, I., et al. 2010, "Wavelength Calibration Accuracy for the STIS CCD and MAMA Modes", ISR STIS 2011-01(v1).

Shaw, D., Kaiser, M.E., & Ferguson, H. 1998, "MAMA Flat-field Status and Plans", ISR STIS 98-15.

Zheng, W., et al. 2011, "Dark Rate of the STIS NUV detector", ISR STIS 2011-03.

6. Appendix

Table 4 lists the STIS reference files delivered as part of analysis of data taken in Cycle 18 calibration programs. However, it excludes regular darks and biases delivered monthly from programs 12401, 12402, 12403, and 12404. Table 5 lists the instrument science reports and technical instrument reports produced as a result of analysis of Cycle 18 calibration programs.

Table 4. STIS Cycle 18 Reference File Deliveries

Reference File	File type	Delivery Date	Contributing Programs
v2a1855f0_tdc.fits	Dark Correction Table	02/10/2011	12415
v6n13233o_ccd.fits	CCD Parameters Table	06/23/2011	12396, 12408
w521257ro_pfl.fits	Pixel-to-pixel flatfield image	05/02/2012	12405
w5212581o_pfl.fits	Pixel-to-pixel flatfield image	05/02/2012	12405
w521257to_pfl.fits	Pixel-to-pixel flatfield image	05/02/2012	12405
w5212580o_pfl.fits	Pixel-to-pixel flatfield image	05/02/2012	12405
w521257qo_pfl.fits	Pixel-to-pixel flatfield image	05/02/2012	12405
w521257so_pfl.fits	Pixel-to-pixel flatfield image	05/02/2012	12405

Table 5. Instrument Science Reports & Technical Instrument Reports Produced from Cycle 18 Calibration Programs

Number	Contributing Programs	First Author	Title
ISR STIS 2011-03	12415	Wei Zheng	"Dark Rate of the STIS NUV detector"
ISR STIS 2013-02	12409 & 12413	Julia Roman-Duval	"Full-field sensitivity and its time-dependence for the STIS CCD and MAMAs"
ISR STIS 2013-05	12405	Elena Mason	"STIS CCD Spectroscopic P-flats"